

# Small-Coupling Dynamic Cavity: a Bayesian mean-field framework for epidemic inference

Alfredo Braunstein,<sup>1,2,3</sup> Giovanni Catania,<sup>4</sup> Luca Dall'Asta,<sup>1,3,\*</sup>  
Matteo Mariani,<sup>1</sup> Fabio Mazza,<sup>1</sup> and Mattia Tarabolo<sup>1</sup>

<sup>1</sup>*Institute of Condensed Matter Physics and Complex Systems,  
Department of Applied Science and Technology, Politecnico di Torino,  
C.so Duca degli Abruzzi 24, 10129 Torino, Italy*

<sup>2</sup>*Italian Institute for Genomic Medicine (IIGM) and Candiolo Cancer Institute IRCCS,  
str. prov. 142, km 3.95, Candiolo (TO) 10060, Italy*

<sup>3</sup>*Collegio Carlo Alberto, Piazza Arbarello 8, 10122, Torino, Italy*

<sup>4</sup>*Departamento de Física Téorica, Universidad Complutense, 28040 Madrid, Spain*

A novel generalized mean field approximation, called the Small-Coupling Dynamic Cavity (SCDC) method, for epidemic inference and risk assessment is presented. The method is developed within a fully Bayesian framework and accounts for non-causal effects generated by the presence of observations. It is based on a graphical model representation of the epidemic stochastic process and utilizes dynamic cavity equations to derive a set of self-consistent equations for probability marginals defined on the edges of the contact graph. By performing a small-coupling expansion, a pair of time-dependent cavity messages is obtained, which capture the probability of individual infection and the conditioning power of observations. In its efficient formulation, the computational cost per iteration of the SCDC algorithm is linear in the duration of the epidemic dynamics and in the number of contacts. The SCDC method is derived for the Susceptible-Infected (SI) model and straightforwardly applicable to other Markovian epidemic processes, including recurrent ones. It exhibits high accuracy in assessing individual risk on par with Belief Propagation techniques and outperforming heuristic methods based on individual-based mean-field approximations. Although convergence issues may arise due to long-range correlations in contact graphs, the estimated marginal probabilities remain sufficiently accurate for reliable risk estimation. Future work includes extending the method to non-Markovian recurrent epidemic models and investigating the role of second-order terms in the small coupling expansion of the observation-reweighted Dynamic Cavity equations.

## I. INTRODUCTION

In the past decade, the increasing availability of detailed epidemiological data and high-accuracy contact-network datasets triggered the study of individual-based epidemic inference problems. The interest has been further stimulated during the COVID-19 pandemic, by the possibility of performing massive epidemic surveillance and digital contact tracing via smartphone applications [1, 2]. A variety of computational methods were proposed for tackling this class of inference problems, such as heuristic algorithms based on network centrality measures [3, 4], generalized mean-field approximations [5], Monte Carlo methods [6], and machine learning techniques exploiting tailored architectures of autoregressive and graph neural networks [7–11]. The leading technique for epidemic inference adopts a Bayesian framework, with a simple individual-based epidemic model as prior distribution and the sparse observation of positive/negative test results as evidence, and consists of an efficient message-passing algorithm based on a Belief Propagation (BP) approximation of the posterior distribution [12–15]. The method has proved to be extremely effective in estimating local marginal probabilities of the posterior distribution, reconstructing the infection state of unobserved individuals, and identifying patient zero and contagion channels. Furthermore, when integrated into the framework of digital contact tracing for COVID-19, the BP-based algorithms have been shown to provide a better assessment of individual risk and improve the mitigation impact of non-pharmaceutical intervention strategies, outperforming competing methods for various epidemic inference problems defined on contact networks [2].

The Belief Propagation approach to spatio-temporal epidemic trajectories can be classified as a generalized mean-field method because the epidemic trajectories of the neighbors of a given individual are assumed to be conditionally independent. This hypothesis is correct when the dynamical process takes place on a contact network without cycles, but the method proved to be very effective also on contact networks with cycles. This is the same assumption of the Dynamic Cavity (DC) approach [16, 17], which turns out to be equivalent to BP in the case of pure time-forward epidemic dynamics without observations. Moreover, for dynamic models with non-recurrent individual states,

---

\* [luca.dallasta@polito.it](mailto:luca.dallasta@polito.it)

in the case of pure time-forward epidemic dynamics without observations, the BP/DC approach simplifies into a dynamic message passing technique that has been extensively used to study spreading processes on networks [18, 19]. Even simpler individual-based mean-field (IBMF) methods, also known as quenched mean-field and  $N$ -intertwined models, which assume that the states of neighboring nodes are statistically independent, have been shown to provide moderately good approximations to time-forward epidemic dynamics [20–23]. Recently, the individual-based mean-field method has been employed to propose a very simple inference method where the observations of individual states are heuristically taken into account [2]. Unlike the absence of a correct Bayesian framework and the simplicity of the approach, this method provides moderately good results for epidemic risk assessment.

In this paper, a novel generalized mean field approximation for Bayesian epidemic inference and risk assessment is proposed. The starting point of the method is a graphical model representation of the epidemic stochastic process that allows for a convenient derivation of a set of dynamic cavity equations for functional probability marginals defined on the edges of the contact graph. In this representation, the cavity probability marginal on a directed edge from individual  $i$  to individual  $j$  is a function of two quantities: the trajectory of the individual state of  $i$  in the absence of interactions with  $j$  and a conjugate external field acting on  $i$  (which replaces the effect of the missing interaction terms in the cavity graph). By performing an expansion of the dynamic cavity equations for weak infection probabilities and truncating the expansion at the first order, a set of self-consistent equations for the average of these two quantities can be obtained. This Small-Coupling Dynamic Cavity (SCDC) method is expected to be less accurate than BP for epidemic trajectories, for which it represents a sort of weak-infectivity approximation. Despite most common heuristic methods based on centrality measures and individual-based mean-field approximations, the proposed method is developed within a fully Bayesian formulation and accounts for non-causal effects generated by the presence of observations. In the absence of observations, the conjugate fields responsible for non-causal dynamics vanish, and the individual-based mean-field method for time-forward dynamics can be recovered. For clarity, the SCDC method is developed in the case of the Susceptible-Infected model, for which efficient computational schemes can be easily devised. Using an efficient formulation based on a transfer-matrix technique, the SCDC method can be straightforwardly extended to more general Markovian epidemic processes, including individual recovery, latency, and recurrent infection (e.g. SIR, SEIR, SIS, SIRS models).

The manuscript is organized as follows: Section II presents the SCDC method and its derivation on the SI model; Section III discusses a general efficient formulation of the algorithm that is easy to generalize to other epidemic models (further discussed in Section IV); results are presented in Section V, concerning both estimates of epidemic outbreaks in the absence of observations and individual risk assessment from partial observations, on both irreversible and recurrent compartmental models; finally, Section VI draws the conclusions and highlights future directions to be investigated.

## II. METHODOLOGY

### A. Definition of the stochastic epidemic model and observations

The simplest non-trivial model employed in epidemic inference is the discrete-time stochastic Susceptible-Infected (SI) model. The application of the proposed method to more general epidemic models is discussed in Section IV. It is thus considered the dynamics of the SI model on a population of  $N$  individuals over a temporal window of  $T$  time steps (e.g. days). The daily contacts are directly encoded in the set of parameters specifying the infection transmission, with  $\lambda_{ij}^t$  being the infection probability along the directed edge from individual  $i$  to individual  $j$  at time  $t$ ; conversely, we set  $\lambda_{ij}^t = \lambda_{ji}^t = 0$  if  $i$  and  $j$  are not in contact at time  $t$ . The epidemic state of the population at time  $t$  is represented by a binary array  $\mathbf{x}^t = (x_1^t, \dots, x_N^t)$ , with  $x_i^t = 0$  (resp.  $x_i^t = 1$ ) meaning that  $i$  is a Susceptible (resp. Infected) individual at time  $t$ . For the sake of generality we include in the model a small self-infection probability  $\varepsilon_i^t$ . The epidemic model is assumed to be Markovian, although this hypothesis can be relaxed. In the Markovian setup, the time evolution of the probability  $p_t[\mathbf{x}^t]$  that the population is in state  $\mathbf{x}^t$  at time  $t$  is given in terms of the following master equation

$$p_{t+1}[\mathbf{x}^{t+1}] = \sum_{\mathbf{x}^t} W[\mathbf{x}^{t+1}|\mathbf{x}^t] p_t[\mathbf{x}^t], \quad (1)$$

with transition rates  $W[\mathbf{x}^{t+1}|\mathbf{x}^t] = \prod_i W_i(x_i^{t+1}|\mathbf{x}^t)$  where

$$W_i(x_i^{t+1} = 1|\mathbf{x}^t) = x_i^t + (1 - x_i^t) \left[ 1 - (1 - \varepsilon_i^t) \prod_j (1 - \lambda_{ji}^t x_j^t) \right], \quad (2a)$$

$$W_i(x_i^{t+1} = 0|\mathbf{x}^t) = (1 - x_i^t) (1 - \varepsilon_i^t) \prod_j (1 - \lambda_{ji}^t x_j^t). \quad (2b)$$

It is convenient to introduce a set of local fields  $h_i^t = \sum_j \nu_{ji}^t x_j^t$ , with  $\nu_{ji}^t = \log(1 - \lambda_{ji}^t)$ , such that

$$\prod_j (1 - \lambda_{ji}^t x_j^t) = \prod_j (1 - \lambda_{ji}^t)^{x_j^t} = e^{h_i^t}, \quad (3)$$

and use them to provide an equivalent description to the master equation (1), based on a system of discrete-time stochastic maps

$$x_i^{t+1} = x_i^t + (1 - x_i^t) y_i^t, \quad (4)$$

in which  $y_i^t$  is a Bernoulli random variable with parameter  $1 - e^{h_i^t} (1 - \varepsilon_i^t)$ , i.e.

$$P[y_i^t | h_i^t] = \text{Bernoulli}\left(1 - e^{h_i^t} (1 - \varepsilon_i^t)\right). \quad (5)$$

The likelihood of the model can be defined by a set  $\mathcal{O}$  of statistically independent observations, each of them providing information about the state of a certain node  $i$  at the corresponding observation time. The most general scenario admits multiple observations on the same node  $i$  (at different times), encoded in the vectors  $\mathbf{O}_i$ , and uncertainty on the outcome of the tests, the latter being eventually quantified by false positive rate  $f_{\text{FPR}}$  and/or false negative rates  $f_{\text{FNR}}$ . If node  $i$  is observed at time  $\tau_{o_i}$ , the corresponding likelihood over its epidemic trajectory  $\mathbf{x}_i = (x_i^0, \dots, x_i^T)$  reads

$$p(\mathbf{O}_i^{\tau_{o_i}} | \mathbf{x}_i) = \begin{cases} (1 - f_{\text{FPR}}) \delta_{x_i^{\tau_{o_i}}, 0} + f_{\text{FNR}} \delta_{x_i^{\tau_{o_i}}, 1} & \text{if } O_i^{\tau_{o_i}} = 0 \\ f_{\text{FPR}} \delta_{x_i^{\tau_{o_i}}, 0} + (1 - f_{\text{FNR}}) \delta_{x_i^{\tau_{o_i}}, 1} & \text{if } O_i^{\tau_{o_i}} = 1 \end{cases} \quad (6)$$

where  $\delta_{x,y}$  denotes the Kronecker symbol. The total likelihood over the full set of observations  $\mathcal{O} = \{\mathbf{O}_i\}_{i=1}^N$  can be rewritten as

$$p(\mathcal{O} | \mathbf{X}) = \prod_i p(\mathbf{O}_i | \mathbf{x}_i) = \prod_i \prod_{o_i \in \mathbf{O}_i} p(O_i^{\tau_{o_i}} | \mathbf{x}_i), \quad (7)$$

where each term in the last equation takes the form given in (6). At the rightmost-hand side, the second product runs over all the observations  $\mathbf{O}_i$  on node  $i$ . In the above equation the quantity  $\mathbf{X}$  is a short-hand notation to indicate the trajectories of all nodes, namely  $\mathbf{X} = \{\mathbf{x}_1, \mathbf{x}_2, \dots, \mathbf{x}_N\} = \{\mathbf{x}^0, \mathbf{x}^1, \dots, \mathbf{x}^T\}$ . In the case of perfectly accurate tests, in which  $f_{\text{FPR}} = f_{\text{FNR}} = 0$ , the effect of the observations is to enforce the dynamical trajectories to be compatible with the observed states. The posterior probability of the trajectory  $\mathbf{X}$  can be expressed using Bayes' theorem as follows

$$p(\mathbf{X}|\mathcal{O}) = \frac{1}{p(\mathcal{O})} p(\mathbf{X}) p(\mathcal{O} | \mathbf{X}) \quad (8a)$$

$$= \frac{1}{p(\mathcal{O})} \prod_{i=1}^N \left\{ p(x_i^0) \prod_{t=0}^{T-1} \left[ \sum_{y_i^t} \int dh_i^t P[y_i^t | h_i^t] \delta_{x_i^{t+1}, x_i^t + (1-x_i^t)y_i^t} \delta \left( h_i^t - \sum_j \nu_{ji}^t x_j^t \right) \right] \right\} p(\mathbf{O}_i | \mathbf{x}_i) \quad (8b)$$

$$\propto \prod_i \left\{ p(x_i^0) \prod_{t=0}^{T-1} \left[ \sum_{y_i^t} \int dh_i^t P[y_i^t | h_i^t] \delta_{x_i^{t+1}, x_i^t + (1-x_i^t)y_i^t} \delta \left( h_i^t - \sum_j \nu_{ji}^t x_j^t \right) p(O_i^t | x_i^t) \right] \right\} p(O_i^T | x_i^T), \quad (8c)$$

where in the last expression it is assumed the simplifying notation that the conditional probability  $p(O_i^t | x_i^t) = 1$  also in the case in which there is no observation of the state of individual  $i$  at time  $t$ , i.e.  $\nexists o_i$  such that  $t = \tau_{o_i}$ . The

same will be assumed in the rest of the paper. Alternatively, by summing over the variables  $y_i^t$  and  $h_i^t$  for all  $i$  and  $t$ , Eq.(8c) becomes

$$p(\mathbf{X}|\mathcal{O}) \propto \prod_i \left\{ p(x_i^0) \prod_{t=0}^{T-1} \left[ \delta_{x_i^{t+1}, x_i^t} (1 - \varepsilon_i^t) e^{\sum_{k \in \partial_i} \nu_{ki}^t x_k^t} + \delta_{x_i^{t+1}, 1} \left( 1 - (1 - \varepsilon_i^t) e^{\sum_{k \in \partial_i} \nu_{ki}^t x_k^t} \right) \right] p(O_i^t | x_i^t) \right\} p(O_i^T | x_i^T), \quad (9)$$

The Bayesian inference problem consists in evaluating marginals of the posterior distribution  $p(\mathbf{X}|\mathcal{O})$ , such as the quantity  $p(x_i^t = x | \mathcal{O})$  representing the posterior probability that individual  $i$  is in state  $x \in \{0, 1\}$  at time  $t$  given the set of the available observations  $\mathcal{O}$ . The posterior distribution is, in general, intractable but it is the starting point for the derivation of approximate inference methods.

## B. The Dynamic Cavity Equations for the SI model with observations

The posterior probability in Eq.(9) can be interpreted as a graphical model for dynamical trajectories defined on the contact network, for which a Belief Propagation approach was first proposed in Refs. [12, 13]. In particular, defining variable nodes grouping together pairs of dynamical trajectories for neighboring nodes, the short loops naturally introduced by the dynamical constraints can be disentangled, leading to the following set of *Belief Propagation (BP) equations* [12, 13],

$$c_{ij}^{\text{BP}}[\mathbf{x}_i, \mathbf{x}_j | \mathcal{O}] \propto p(x_i^0) \sum_{\mathbf{x}_{\partial i \setminus j}} \left\{ \left[ \prod_{k \in \partial i \setminus j} c_{ki}^{\text{BP}}[\mathbf{x}_k, \mathbf{x}_i | \mathcal{O}] \right] p(O_i^T | x_i^T) \right. \\ \left. \times \prod_{t=0}^{T-1} \left[ \delta_{x_i^{t+1}, x_i^t} (1 - \varepsilon_i^t) e^{\sum_{k \in \partial_i} \nu_{ki}^t x_k^t} + \delta_{x_i^{t+1}, 1} \left( 1 - (1 - \varepsilon_i^t) e^{\sum_{k \in \partial_i} \nu_{ki}^t x_k^t} \right) \right] p(O_i^t | x_i^t) \right\}, \quad (10)$$

where  $\mathbf{x}_{\partial i \setminus j} = \{\mathbf{x}_k\}_{k \in \partial i \setminus j}$  is the set of trajectories on neighbors of  $i$  except for  $j$  and  $c_{ij}^{\text{BP}}[\mathbf{x}_i, \mathbf{x}_j | \mathcal{O}]$  are the BP messages depending on the trajectories of the nodes  $i$  and  $j$  (at given observation set  $\mathcal{O}$ ). The BP equations are exact when the underlying interaction graph (the time-independent projection of the contact network) is a tree and provide a rather good approximation of the posterior distribution on sparse loopy graphs.

An equivalent formulation can be obtained starting from the posterior probability in Eq. (8c), employing a cavity argument by removing the node  $j$  (and the corresponding trajectory  $\mathbf{x}_j = (x_j^0, \dots, x_j^T)$ ) and deriving a set of equations for the marginal probability  $c_{ij}[\mathbf{x}_i, \mathbf{s}_i | \mathcal{O}]$ , that represents the probability of the pair of variable-field trajectories  $(\mathbf{x}_i, \mathbf{s}_i)$  on node  $i$  in the cavity graph. In this way (see Appendix A for a full derivation from Eq. (8c)), the following *observation-reweighted dynamic cavity (DC) equations* can be obtained

$$c_{ij}[\mathbf{x}_i, \mathbf{s}_i | \mathcal{O}] = \frac{1}{Z_{ij}[\mathcal{O}]} p(x_i^0) \sum_{\mathbf{x}_{\partial i \setminus j}} \left\{ \left[ \prod_{k \in \partial i \setminus j} c_{ki}[\mathbf{x}_k, \boldsymbol{\nu}_{ik} \mathbf{x}_i | \mathcal{O}] \right] p(O_i^T | x_i^T) \right. \\ \left. \times \prod_{t=0}^{T-1} \left[ \delta_{x_i^{t+1}, x_i^t} (1 - \varepsilon_i^t) e^{s_i^t + \sum_{k \in \partial i \setminus j} \nu_{ki}^t x_k^t} + \delta_{x_i^{t+1}, 1} \left( 1 - (1 - \varepsilon_i^t) e^{s_i^t + \sum_{k \in \partial i \setminus j} \nu_{ki}^t x_k^t} \right) \right] p(O_i^t | x_i^t) \right\}, \quad (11)$$

where the notation  $\boldsymbol{\nu}_{ik} \mathbf{x}_i$  stands for the array  $(\nu_{ik}^1 x_i^1, \dots, \nu_{ik}^T x_i^T)$ , and  $Z_{ij}[\mathcal{O}]$  is a normalization term for the cavity marginals. While the dynamic cavity equations with variable-field trajectories were originally proposed only for time-forward binary spin dynamics in Refs. [16, 17], those in Eqs.(11) also account for probabilistic reweighting due to the observations.

Since the two representations in Eqs.(10) and (11) are equivalent, it is convenient to interpret  $\mathbf{s}_i$  in the cavity marginal  $c_{ij}[\mathbf{x}_i, \mathbf{s}_i | \mathcal{O}]$  as a proxy for the trajectory of the missing neighboring node  $j$  in the cavity graph (more precisely  $\mathbf{s}_i \propto \boldsymbol{\nu}_{ji} \mathbf{x}_j$ ), essentially recovering in this way the BP cavity marginal  $c_{ij}^{\text{BP}}[\mathbf{x}_i, \mathbf{x}_j | \mathcal{O}]$ . It appears then an arbitrary but natural choice to normalize the marginals by tracing over both arguments, by defining

$$Z_{ij}[\mathcal{O}] = \sum_{\mathbf{x}_i, \mathbf{s}_i} p(x_i^0) \sum_{\mathbf{x}_{\partial i \setminus j}} \left\{ \left[ \prod_{k \in \partial i \setminus j} c_{ki}[\mathbf{x}_k, \boldsymbol{\nu}_{ik} \mathbf{x}_i | \mathcal{O}] \right] \prod_{t=0}^{T-1} \left[ \delta_{x_i^{t+1}, x_i^t} (1 - \varepsilon_i^t) e^{s_i^t + \sum_{k \in \partial i \setminus j} \nu_{ki}^t x_k^t} \right. \right. \\ \left. \left. + \delta_{x_i^{t+1}, 1} \left( 1 - (1 - \varepsilon_i^t) e^{s_i^t + \sum_{k \in \partial i \setminus j} \nu_{ki}^t x_k^t} \right) \right] p(O_i^t | x_i^t) \right\} p(O_i^T | x_i^T). \quad (12)$$

With this choice of normalization, the sum over  $\mathbf{s}_i$  has to run only over field trajectories that are consistent with realizations of the epidemic trajectories  $\nu_{ji}; \mathbf{x}_j$  of the neighboring node  $j$ . It can be alternatively convenient to normalize the cavity marginal only over  $\mathbf{x}_i$  at a fixed realization of the field  $\mathbf{s}_i$ . This is done in Section II C, with a simplifying choice which however will have non-trivial consequences.

Finally, completing the cavity and computing the total marginal over  $i$  gives the posterior marginal probability of one-site trajectories

$$p_i(\mathbf{x}_i | \mathcal{O}) \propto p(x_i^0) \sum_{\mathbf{x}_{\partial i}} \left\{ \left[ \prod_{k \in \partial i} c_{ki}[\mathbf{x}_k, \nu_{ik} \mathbf{x}_i | \mathcal{O}] \right] \prod_{t=0}^{T-1} \left[ \delta_{x_i^{t+1}, x_i^t} (1 - \varepsilon_i^t) e^{\sum_{k \in \partial i} \nu_{ki}^t x_k^t} \right. \right. \\ \left. \left. + \delta_{x_i^{t+1}, 1} \left( 1 - (1 - \varepsilon_i^t) e^{\sum_{k \in \partial i} \nu_{ki}^t x_k^t} \right) \right] p(O_i^t | x_i^t) \right\} p(O_i^T | x_i^T). \quad (13)$$

### C. Small-coupling expansion

It is convenient to express the cavity marginal in Eq. (11) in terms of the conjugate field trajectory  $\hat{\mathbf{h}}_i = (\hat{h}_i^1, \dots, \hat{h}_i^T)$ , by introducing its Fourier transform (see Appendix A), which leads to the following expression for the dynamic cavity equations

$$c_{ij}[\mathbf{x}_i, \hat{\mathbf{h}}_i | \mathcal{O}] = \frac{p(x_i^0)}{\mathcal{Z}_{ij}[\mathcal{O}]} \prod_{t=0}^{T-1} \left\{ \left[ \delta(\hat{h}_i^t - i) (1 - \varepsilon_i^t) \left( \delta_{x_i^{t+1}, x_i^t} - \delta_{x_i^{t+1}, 1} \right) + \delta(\hat{h}_i^t) \delta_{x_i^{t+1}, 1} \right] p(O_i^t | x_i^t) \right\} \\ \times \prod_{k \in \partial i \setminus j} \left[ \sum_{\mathbf{x}_k} \int D\hat{\mathbf{h}}_k c_{ki}[\mathbf{x}_k, \hat{\mathbf{h}}_k | \mathcal{O}] e^{-i \sum_t (x_k^t \nu_{ki}^t \hat{h}_i^t + x_i^t \nu_{ik}^t \hat{h}_k^t)} \right] p(O_i^T | x_i^T), \quad (14)$$

in which the choice of normalization  $\mathcal{Z}_{ij}[\mathcal{O}]$  will be discussed later.

In the spirit of Plefka's approach [24, 25] and high-temperature expansions [26, 27], one can perform a formal expansion of the exponential term. Since the argument of the exponential is linear in the parameters  $\nu_{ik}^t$  and  $\nu_{ki}^t$ , truncating the expansion at some finite order can be understood as a small-coupling approximation of the dynamic cavity equations, which in the case of epidemic processes corresponds to a small infectivity approximation (i.e.  $\lambda_{ij}^t \ll 1$  for all  $i, j$  and  $t$ ). Truncating the Taylor series at the second order, we get

$$c_{ij}[\mathbf{x}_i, \hat{\mathbf{h}}_i | \mathcal{O}] = \frac{p(x_i^0)}{\mathcal{Z}_{ij}[\mathcal{O}]} \prod_{t=0}^{T-1} \left\{ \left[ \delta(\hat{h}_i^t - i) (1 - \varepsilon_i^t) \left( \delta_{x_i^{t+1}, x_i^t} - \delta_{x_i^{t+1}, 1} \right) + \delta(\hat{h}_i^t) \delta_{x_i^{t+1}, 1} \right] p(O_i^t | x_i^t) \right\} \\ \times \prod_{k \in \partial i \setminus j} \left[ \sum_{\mathbf{x}_k} \int D\hat{\mathbf{h}}_k c_{ki}[\mathbf{x}_k, \hat{\mathbf{h}}_k | \mathcal{O}] e^{-i \sum_t (x_k^t \nu_{ki}^t \hat{h}_i^t + x_i^t \nu_{ik}^t \hat{h}_k^t)} \right] p(O_i^T | x_i^T) \quad (15a)$$

$$\approx \frac{p(x_i^0)}{\mathcal{Z}_{ij}[\mathcal{O}]} \prod_{t=0}^{T-1} \left\{ \left[ \delta(\hat{h}_i^t - i) (1 - \varepsilon_i^t) \left( \delta_{x_i^{t+1}, x_i^t} - \delta_{x_i^{t+1}, 1} \right) + \delta(\hat{h}_i^t) \delta_{x_i^{t+1}, 1} \right] p(O_i^t | x_i^t) \right\} \\ \times \prod_{k \in \partial i \setminus j} \sum_{\mathbf{x}_k} \int D\hat{\mathbf{h}}_k c_{ki}[\mathbf{x}_k, \hat{\mathbf{h}}_k | \mathcal{O}] \left\{ 1 - i \sum_t \left( x_k^t \nu_{ki}^t \hat{h}_i^t + x_i^t \nu_{ik}^t \hat{h}_k^t \right) \right. \\ \left. + \frac{1}{2} \sum_{t, t'} \left( x_k^t \nu_{ki}^t (-i \hat{h}_i^t) + x_i^t \nu_{ik}^t (-i \hat{h}_k^t) \right) \left( x_k^{t'} \nu_{ki}^{t'} (-i \hat{h}_i^{t'}) + x_i^{t'} \nu_{ik}^{t'} (-i \hat{h}_k^{t'}) \right) \right\} p(O_i^T | x_i^T), \quad (15b)$$

where also the normalization constant is consistently approximated. In order to perform the averages over the dynamic cavity marginals  $c_{ki}$ , we choose the normalization  $\mathcal{Z}_{ij}[\mathcal{O}]$  in such a way that

$$\sum_{\mathbf{x}_i} \int D\hat{\mathbf{h}}_i c_{ij}[\mathbf{x}_i, \hat{\mathbf{h}}_i | \mathcal{O}] = \sum_{\mathbf{x}_i} c_{ij}[\mathbf{x}_i, \mathbf{s}_i = 0 | \mathcal{O}] = 1 \quad (16)$$

which is equivalent to assume that the neighboring individual  $j$  stays in the susceptible state at all times. Choosing the normalization to be independent of the trajectory of individual  $j$  is highly advantageous for developing an

approximation that does not explicitly rely on the epidemic trajectories of both  $i$  and  $j$ . However, this choice has the consequence that some particular epidemic trajectories of individual  $i$ , imposed by the observations, can only be explained by the statistical model if a non-zero self-infection probability is introduced. In Appendix E, we provide an example of this potential issue that is simple enough to be discussed analytically and show how the presence of a self-infection probability effectively resolves it. It is now possible to explicitly perform the averages over the dynamic cavity marginals  $c_{ki}$ , obtaining

$$\begin{aligned}
c_{ij} [\mathbf{x}_i, \hat{\mathbf{h}}_i | \mathcal{O}] &\approx \frac{p(x_i^0)}{\mathcal{Z}_{ij}[\mathcal{O}]} \prod_{t=0}^{T-1} \left\{ \left[ \delta(\hat{h}_i^t - i) (1 - \varepsilon_i^t) (\delta_{x_i^{t+1}, x_i^t} - \delta_{x_i^{t+1}, 1}) + \delta(\hat{h}_i^t) \delta_{x_i^{t+1}, 1} \right] p(O_i^t | x_i^t) \right\} p(O_i^T | x_i^T) \\
&\times \prod_{k \in \partial i \setminus j} \left[ 1 + \sum_t \left( m_{k \setminus i}^t \nu_{ki}^t (-i \hat{h}_i^t) + x_i^t \nu_{ik}^t \mu_{k \setminus i}^t \right) \right. \\
&\quad \left. + \frac{1}{2} \sum_{t, t'} \left[ \nu_{ki}^t (-i \hat{h}_i^t) \nu_{ki}^{t'} (-i \hat{h}_i^{t'}) C_{k \setminus i}^{tt'} + \nu_{ki}^t (-i \hat{h}_i^t) R_{k \setminus i}^{tt'} x_i^{t'} \nu_{ik}^{t'} + \nu_{ki}^{t'} (-i \hat{h}_i^{t'}) R_{k \setminus i}^{t't} x_i^t \nu_{ik}^t + B_{k \setminus i}^{tt'} x_i^t \nu_{ik}^t x_i^{t'} \nu_{ik}^{t'} \right] \right]
\end{aligned} \tag{17}$$

in which a set of one-time and two-time cavity quantities were defined by the relations

$$\begin{aligned}
m_{k \setminus i}^t &= m_{k \setminus i}^t[\mathcal{O}] = \sum_{\mathbf{x}_k} \int D\hat{\mathbf{h}}_k c_{ki} [\mathbf{x}_k, \hat{\mathbf{h}}_k | \mathcal{O}] x_k^t \\
&= \sum_{\mathbf{x}_k} c_{ki} [\mathbf{x}_k, \mathbf{s}_k = 0 | \mathcal{O}] x_k^t,
\end{aligned} \tag{18}$$

$$\begin{aligned}
\mu_{k \setminus i}^t &= \mu_{k \setminus i}^t[\mathcal{O}] = \sum_{\mathbf{x}_k} \int D\hat{\mathbf{h}}_k c_{ki} [\mathbf{x}_k, \hat{\mathbf{h}}_k | \mathcal{O}] (-i \hat{h}_k^t) \\
&= \sum_{\mathbf{x}_k} \frac{\delta}{\delta s_k^t} c_{ki} [\mathbf{x}_k, \mathbf{s}_k | \mathcal{O}] \Big|_{s_k=0},
\end{aligned} \tag{19}$$

and

$$\begin{aligned}
C_{k \setminus i}^{tt'} &= C_{k \setminus i}^{t, t'}[\mathcal{O}] = \sum_{\mathbf{x}_k} \int D\hat{\mathbf{h}}_k c_{ki} [\mathbf{x}_k, \hat{\mathbf{h}}_k | \mathcal{O}] x_k^t x_k^{t'} \\
&= \sum_{\mathbf{x}_k} c_{ki} [\mathbf{x}_k, \mathbf{s}_k = 0 | \mathcal{O}] x_k^t x_k^{t'},
\end{aligned} \tag{20}$$

$$\begin{aligned}
R_{k \setminus i}^{tt'} &= R_{k \setminus i}^{t, t'}[\mathcal{O}] = \sum_{\mathbf{x}_k} \int D\hat{\mathbf{h}}_k c_{ki} [\mathbf{x}_k, \hat{\mathbf{h}}_k | \mathcal{O}] x_k^t (-i \hat{h}_k^{t'}) \\
&= \frac{\delta}{\delta s_k^{t'}} \sum_{\mathbf{x}_k} x_k^t c_{ki} [\mathbf{x}_k, \mathbf{s}_k | \mathcal{O}] \Big|_{s_k=0},
\end{aligned} \tag{21}$$

$$\begin{aligned}
B_{k \setminus i}^{tt'} &= B_{k \setminus i}^{t, t'}[\mathcal{O}] = \sum_{\mathbf{x}_k} \int D\hat{\mathbf{h}}_k c_{ki} [\mathbf{x}_k, \hat{\mathbf{h}}_k | \mathcal{O}] (-i \hat{h}_k^t) (-i \hat{h}_k^{t'}) \\
&= \frac{\delta^2}{\delta s_k^t \delta s_k^{t'}} \sum_{\mathbf{x}_k} c_{ki} [\mathbf{x}_k, \mathbf{s}_k | \mathcal{O}] \Big|_{s_k=0}.
\end{aligned} \tag{22}$$

Finally, we get the following approximated form of the equations

$$\begin{aligned}
c_{ij} [\mathbf{x}_i, \hat{\mathbf{h}}_i | \mathcal{O}] &= \frac{p(x_i^0)}{\tilde{\mathcal{Z}}_{ij}[\mathcal{O}]} \prod_{t=0}^{T-1} \left\{ \left[ \delta(\hat{h}_i^t - i) (1 - \varepsilon_i^t) (\delta_{x_i^{t+1}, x_i^t} - \delta_{x_i^{t+1}, 1}) + \delta(\hat{h}_i^t) \delta_{x_i^{t+1}, 1} \right] p(O_i^t | x_i^t) \right\} p(O_i^T | x_i^T) \\
&\times \prod_t \exp \left\{ \sum_{k \in \partial i \setminus j} \left( m_{k \setminus i}^t \nu_{ki}^t (-i \hat{h}_i^t) + x_i^t \nu_{ik}^t \mu_{k \setminus i}^t \right) \right. \\
&\quad \left. + \frac{1}{2} \sum_{k \in \partial i \setminus j} \sum_{t'} \left[ -\nu_{ki}^t \hat{h}_i^t \nu_{ki}^{t'} \hat{h}_i^{t'} C_{k \setminus i}^{tt'} - i \hat{h}_i^t \nu_{ki}^t R_{k \setminus i}^{tt'} x_i^{t'} \nu_{ik}^{t'} - i \hat{h}_i^{t'} \nu_{ki}^{t'} R_{k \setminus i}^{tt'} x_i^t \nu_{ik}^t + B_{k \setminus i}^{tt'} x_i^t \nu_{ik}^t x_i^{t'} \nu_{ik}^{t'} \right] \right\}, \tag{23}
\end{aligned}$$

where  $\tilde{\mathcal{Z}}_{ij}[\mathcal{O}]$  is the normalization constant of the re-exponentiated form of the equations.

The quantity  $m_{k \setminus i}^t$  measures the average probability that node  $k$  is infected at time  $t$  in the absence of the interaction with  $i$ . Similarly,  $C_{k \setminus i}^{tt'}$  represents the two-time autocorrelation function of node  $k$  in the cavity graph; the quantity  $R_{k \setminus i}^{tt'}$  is the response function on node  $k$  at time  $t'$  to a perturbation due to an infinitesimal external field acting on node  $k$  at time  $t'$ . The remaining two quantities  $\mu_{k \setminus i}^t$  and  $B_{k \setminus i}^{tt'}$  are of less intuitive interpretation, as they measure the mean and temporal correlations of fluctuations around the unperturbed single-site statistics in the cavity graph. A direct calculation of the quantity  $\sum_{\mathbf{x}_k} \int D\hat{\mathbf{h}}_k (-i \hat{h}_k^t) c_{ki}[\mathbf{x}_k, \hat{\mathbf{h}}_k | \mathcal{O} = \emptyset]$  shows that, in the absence of observations,  $\mu_{k \setminus i}^t = 0$ . Similarly,  $B_{k \setminus i}^{tt'} = 0$  in the absence of observations. This result, due to the causality of the dynamical process, does not hold anymore when some observations are included. For notational convenience, the implicit dependence of all marginals and normalization constants on the set of observations  $\mathcal{O}$  will not be further reported in the following.

#### D. Small-Coupling Dynamic Cavity (SCDC) approximation

A straightforward mean-field approximation can be obtained neglecting the second-order terms in Eq. (23) and focusing on the effects of the first-order ones. The expression of the dynamic cavity equations simplifies as follows

$$\begin{aligned}
c_{ij} [\mathbf{x}_i, \mathbf{s}_i] &= \frac{p(x_i^0)}{\tilde{\mathcal{Z}}_{ij}} \prod_{t=0}^{T-1} \left\{ \int d\hat{h}_i^t e^{-i \hat{h}_i^t (s_i^t + \sum_{k \in \partial i \setminus j} m_{k \setminus i}^t \nu_{ki}^t)} \left[ \delta(\hat{h}_i^t - i) (1 - \varepsilon_i^t) (\delta_{x_i^{t+1}, x_i^t} - \delta_{x_i^{t+1}, 1}) \right. \right. \\
&\quad \left. \left. + \delta(\hat{h}_i^t) \delta_{x_i^{t+1}, 1} \right] e^{\sum_{k \in \partial i \setminus j} x_i^t \nu_{ik}^t \mu_{k \setminus i}^t} p(O_i^t | x_i^t) \right\} p(O_i^T | x_i^T) \tag{24a}
\end{aligned}$$

$$\begin{aligned}
&\propto \frac{p(x_i^0)}{\tilde{\mathcal{Z}}_{ij}} \prod_{t=0}^{T-1} \left\{ \left[ \delta_{x_i^{t+1}, x_i^t} (1 - \varepsilon_i^t) e^{s_i^t + \sum_{k \in \partial i \setminus j} m_{k \setminus i}^t \nu_{ki}^t} + \delta_{x_i^{t+1}, 1} \left[ 1 - (1 - \varepsilon_i^t) e^{s_i^t + \sum_{k \in \partial i \setminus j} m_{k \setminus i}^t \nu_{ki}^t} \right] \right] \right\} \\
&\quad \times e^{\sum_{k \in \partial i \setminus j} x_i^t \nu_{ik}^t \mu_{k \setminus i}^t} p(O_i^t | x_i^t) p(O_i^T | x_i^T) \tag{24b}
\end{aligned}$$

where, using the definitions in Eqs. (18) and (19), the two quantities  $m_{i \setminus j}^t$  and  $\mu_{i \setminus j}^t$  turn out to satisfy the self-consistent equations

$$\begin{aligned}
m_{i \setminus j}^t &= \sum_{\mathbf{x}_i} x_i^t \frac{p(x_i^0)}{\tilde{\mathcal{Z}}_{ij}} \prod_{t'=0}^{T-1} \left\{ \left[ \delta_{x_i^{t'+1}, x_i^{t'}} (1 - \varepsilon_i^{t'}) e^{\sum_{k \in \partial i \setminus j} m_{k \setminus i}^{t'} \nu_{ki}^{t'}} + \delta_{x_i^{t'+1}, 1} \left[ 1 - (1 - \varepsilon_i^{t'}) e^{\sum_{k \in \partial i \setminus j} m_{k \setminus i}^{t'} \nu_{ki}^{t'}} \right] \right] \right\} \\
&\quad \times e^{\sum_{k \in \partial i \setminus j} x_i^{t'} \nu_{ik}^{t'} \mu_{k \setminus i}^{t'}} p(O_i^{t'} | x_i^{t'}) p(O_i^T | x_i^T) \tag{25}
\end{aligned}$$

and

$$\begin{aligned}
\mu_{i \setminus j}^t &= \sum_{\mathbf{x}_i} \frac{p(O_i^T | x_i^T) p(x_i^0)}{\tilde{\mathcal{Z}}_{ij}} \\
&\quad \times \prod_{t'=0}^{T-1} \left[ (1 - \delta_{t, t'}) \delta_{x_i^{t'+1}, 1} + (1 - \varepsilon_i^{t'}) (\delta_{x_i^{t'+1}, x_i^{t'}} - \delta_{x_i^{t'+1}, 1}) e^{\sum_{k \in \partial i \setminus j} m_{k \setminus i}^{t'} \nu_{ki}^{t'}} \right] e^{x_i^{t'} \nu_{ik}^{t'} \mu_{k \setminus i}^{t'}} p(O_i^{t'} | x_i^{t'}). \tag{26}
\end{aligned}$$



The normalization constant is chosen to ensure that the time-dependent quantity  $m_{i \setminus j}^t$  represents the mean value of  $x_i^t$  in the cavity graph, that is

$$\begin{aligned} \tilde{Z}_{ij} = & \sum_{\mathbf{x}_i} p(x_i^0) \prod_{t=0}^{T-1} \left[ \left\{ \delta_{x_i^{t+1}, x_i^t} (1 - \varepsilon_i^t) e^{\sum_{k \in \partial i \setminus j} m_{k \setminus i}^t \nu_{ki}^t} + \delta_{x_i^{t+1}, 1} \left[ 1 - (1 - \varepsilon_i^t) e^{\sum_{k \in \partial i \setminus j} m_{k \setminus i}^t \nu_{ki}^t} \right] \right\} \right. \\ & \left. \times e^{\sum_{k \in \partial i \setminus j} x_i^t \nu_{ik}^t \mu_{k \setminus i}^t} p(O_i^t | x_i^t) \right] p(O_i^T | x_i^T). \end{aligned} \quad (27)$$

In addition, the total time-dependent marginal  $m_i^t$  of the posterior distribution on the full graph is given by

$$\begin{aligned} m_i^t = & \frac{1}{\tilde{Z}_i} \sum_{\mathbf{x}_i} p(x_i^0) x_i^t \prod_{t=0}^{T-1} \left[ \left\{ \delta_{x_i^{t+1}, x_i^t} (1 - \varepsilon_i^t) e^{\sum_{k \in \partial i} m_{k \setminus i}^t \nu_{ki}^t} + \delta_{x_i^{t+1}, 1} \left[ 1 - (1 - \varepsilon_i^t) e^{\sum_{k \in \partial i} m_{k \setminus i}^t \nu_{ki}^t} \right] \right\} \right. \\ & \left. \times e^{\sum_{k \in \partial i} x_i^t \nu_{ik}^t \mu_{k \setminus i}^t} p(O_i^t | x_i^t) \right] p(O_i^T | x_i^T) \end{aligned} \quad (28)$$

with

$$\begin{aligned} \tilde{Z}_i = & \sum_{\mathbf{x}_i} p(x_i^0) \prod_{t=0}^{T-1} \left[ \left\{ \delta_{x_i^{t+1}, x_i^t} (1 - \varepsilon_i^t) e^{\sum_{k \in \partial i} m_{k \setminus i}^t \nu_{ki}^t} + \delta_{x_i^{t+1}, 1} \left[ 1 - (1 - \varepsilon_i^t) e^{\sum_{k \in \partial i} m_{k \setminus i}^t \nu_{ki}^t} \right] \right\} \right. \\ & \left. \times e^{\sum_{k \in \partial i} x_i^t \nu_{ik}^t \mu_{k \setminus i}^t} p(O_i^t | x_i^t) \right] p(O_i^T | x_i^T). \end{aligned} \quad (29)$$

Equations (25) and (26) represent a set of self-consistent equations defining a non-causal dynamic mean-field approximation that, in the following, we will refer to as the Small-Coupling Dynamic Cavity (SCDC) method. The dynamical equations are of mean-field type since correlations are neglected, but in the presence of observations, they describe a non-causal dynamical process. Because of the cavity construction, the fundamental unknown of the equations, the one-time cavity marginals  $m_{i \setminus j}^t$  and the one-time cavity fields  $\mu_{i \setminus j}^t$ , are defined by means of local self-consistent conditions, which can be implemented using a message-passing update scheme. A computational bottleneck of Eqs. (25)-(26) is represented by the partial trace over single-site trajectories  $\mathbf{x}_i$ , that requires  $O(2^T)$  operations, meaning that a complete update of all cavity quantities requires  $O(2|E|T2^T)$ , where  $|E|$  is the total number of non-zero weighted directed edges on the interaction graph. An efficient algorithmic implementation of the SCDC equations is proposed in the next Section. It exploits a transfer-matrix approach to perform the trace over the trajectory  $\mathbf{x}_i$  keeping fixed all quantities  $\{m_{k \setminus i}^t\}$  and  $\{\mu_{k \setminus i}^t\}$  for all  $t$  and  $k \in \partial i \setminus j$ , which play the role of the parameters in a “temporal” one-dimensional discrete probabilistic model defined on node  $i$ .

### III. EFFICIENT FORMULATION OF THE SCDC EQUATIONS

The starting point of the derivation is the cavity normalization constant in Eq. (25)-(26), that can be written starting from Eq. (27) as

$$\tilde{Z}_{ij} = \sum_{\mathbf{x}_i} p(x_i^0) \prod_{t=0}^{T-1} M_{x_i^t x_i^{t+1}}^{i \setminus j} (O_i^T | x_i^T) \quad (30)$$

in which  $p(O_i^T | x_i^T) = 1$  if there is no observation at the final time and the “transfer matrix”  $M_{x_i^t x_i^{t+1}}^{i \setminus j}$  is defined as follows

$$M_{x_i^t x_i^{t+1}}^{i \setminus j} = \begin{pmatrix} M_{t,00}^{i \setminus j} & M_{t,01}^{i \setminus j} \\ M_{t,10}^{i \setminus j} & M_{t,11}^{i \setminus j} \end{pmatrix} = \begin{pmatrix} (1 - \varepsilon_i^t) e^{\sum_{k \in \partial i \setminus j} m_{k \setminus i}^t \nu_{ki}^t} p(O_i^t | 0) & \left[ 1 - (1 - \varepsilon_i^t) e^{\sum_{k \in \partial i \setminus j} m_{k \setminus i}^t \nu_{ki}^t} \right] p(O_i^t | 0) \\ 0 & e^{\sum_{k \in \partial i \setminus j} \nu_{ik}^t \mu_{k \setminus i}^t} p(O_i^t | 1) \end{pmatrix} \quad (31)$$

where again it is assumed that  $p(O_i^t | x_i^t) = 1$  if there is no observation on  $i$  at time  $t$ . The probability that an individual  $i$  is infected at time  $t$  in the cavity graph is

$$m_{i \setminus j}^t = \frac{\sum_{x_i^t} \rho_{\rightarrow t}^{i \setminus j}(x_i^t) x_i^t \rho_{t \leftarrow}^{i \setminus j}(x_i^t)}{\sum_{x_i^t} \rho_{\rightarrow t}^{i \setminus j}(x_i^t) \rho_{t \leftarrow}^{i \setminus j}(x_i^t)} = \frac{\rho_{\rightarrow t}^{i \setminus j}(1) \rho_{t \leftarrow}^{i \setminus j}(1)}{\rho_{\rightarrow t}^{i \setminus j}(1) \rho_{t \leftarrow}^{i \setminus j}(1) + \rho_{\rightarrow t}^{i \setminus j}(0) \rho_{t \leftarrow}^{i \setminus j}(0)}, \quad (32)$$



where  $\rho_{\rightarrow t}^{i \setminus j}(x_i^t)$  and  $\rho_{t \leftarrow}^{i \setminus j}(x_i^t)$  are single-site ‘‘temporal’’ messages that satisfy the recursive equations

$$\rho_{\rightarrow t}^{i \setminus j}(x_i^t) = \sum_{x_i^{t-1}} \rho_{\rightarrow t-1}^{i \setminus j}(x_i^{t-1}) M_{x_i^{t-1} x_i^t}^{i \setminus j} \quad \text{for } t \in \{1, \dots, T\} \quad (33a)$$

$$\rho_{t \leftarrow}^{i \setminus j}(x_i^t) = \sum_{x_i^{t+1}} \rho_{t+1 \leftarrow}^{i \setminus j}(x_i^{t+1}) M_{x_i^t x_i^{t+1}}^{i \setminus j} \quad \text{for } t \in \{0, \dots, T-1\}, \quad (33b)$$

and the initial (resp. terminal) conditions are given by  $\rho_{\rightarrow 0}^{i \setminus j}(x_i^0) = p(x_i^0)$  and  $\rho_{T \leftarrow}^{i \setminus j}(x_i^T) = p(O_i^T | x_i^T)$ . The one-time cavity fields  $\mu_{i \setminus j}^t$  can be computed as follows

$$\begin{aligned} \mu_{i \setminus j}^t &= \sum_{x_i} \frac{p(x_i^0)}{\tilde{Z}_{ij}} (1 - \varepsilon_i^t) \left( \delta_{x_i^{t+1}, x_i^t} - \delta_{x_i^{t+1}, 1} \right) e^{\sum_{k \in \partial i \setminus j} (m_{k \setminus i}^t \nu_{ki}^t + x_i^t \nu_{ik}^t \mu_{k \setminus i}^t)} p(O_i^t | x_i^t) \\ &\times \prod_{t' \neq t} \left\{ \delta_{x_i^{t'+1}, x_i^{t'}} (1 - \varepsilon_i^{t'}) e^{\sum_{k \in \partial i \setminus j} m_{k \setminus i}^{t'} \nu_{ki}^{t'} + \delta_{x_i^{t'+1}, 1} \left[ 1 - (1 - \varepsilon_i^{t'}) e^{\sum_{k \in \partial i \setminus j} m_{k \setminus i}^{t'} \nu_{ki}^{t'}} \right]} \right\} \\ &\times e^{\sum_{k \in \partial i \setminus j} x_i^{t'} \nu_{ik}^{t'} \mu_{k \setminus i}^{t'}} p(O_i^{t'} | x_i^{t'}) \Big] p(O_i^T | x_i^T) \end{aligned} \quad (34a)$$

$$= \frac{\sum_{x_i^t, x_i^{t+1}} \rho_{\rightarrow t}^{i \setminus j}(x_i^t) (1 - \varepsilon_i^t) \left( \delta_{x_i^{t+1}, x_i^t} - \delta_{x_i^{t+1}, 1} \right) e^{\sum_{k \in \partial i \setminus j} (m_{k \setminus i}^t \nu_{ki}^t + x_i^t \nu_{ik}^t \mu_{k \setminus i}^t)} p(O_i^t | x_i^t) \rho_{t+1 \leftarrow}^{i \setminus j}(x_i^{t+1})}{\sum_{x_i^t, x_i^{t+1}} \rho_{\rightarrow t}^{i \setminus j}(x_i^t) M_{x_i^t x_i^{t+1}}^{i \setminus j} \rho_{t+1 \leftarrow}^{i \setminus j}(x_i^{t+1})} \quad (34b)$$

$$= \frac{\rho_{\rightarrow t}^{i \setminus j}(0) (1 - \varepsilon_i^t) e^{\sum_{k \in \partial i \setminus j} m_{k \setminus i}^t \nu_{ki}^t} p(O_i^t | 0) \left( \rho_{t+1 \leftarrow}^{i \setminus j}(0) - \rho_{t+1 \leftarrow}^{i \setminus j}(1) \right)}{\sum_{x_i^t, x_i^{t+1}} \rho_{\rightarrow t}^{i \setminus j}(x_i^t) M_{x_i^t x_i^{t+1}}^{i \setminus j} \rho_{t+1 \leftarrow}^{i \setminus j}(x_i^{t+1})} \quad (34c)$$

$$= \frac{\rho_{\rightarrow t}^{i \setminus j}(0) M_{t,00}^{i \setminus j} \left( \rho_{t+1 \leftarrow}^{i \setminus j}(0) - \rho_{t+1 \leftarrow}^{i \setminus j}(1) \right)}{\sum_{x_i^t, x_i^{t+1}} \rho_{\rightarrow t}^{i \setminus j}(x_i^t) M_{x_i^t x_i^{t+1}}^{i \setminus j} \rho_{t+1 \leftarrow}^{i \setminus j}(x_i^{t+1})} \quad (34d)$$

$$= \frac{\rho_{\rightarrow t}^{i \setminus j}(0) M_{t,00}^{i \setminus j} \left( \rho_{t+1 \leftarrow}^{i \setminus j}(0) - \rho_{t+1 \leftarrow}^{i \setminus j}(1) \right)}{\sum_{x_i^t} \rho_{\rightarrow t}^{i \setminus j}(x_i^t) \rho_{t \leftarrow}^{i \setminus j}(x_i^t)}. \quad (34e)$$

The number of operations necessary for the update of a single-time cavity message is now of  $O(1)$  when the single-site ‘‘temporal’’ messages  $\rho_{\rightarrow s}^{i \setminus j}(x_i^s)$  and  $\rho_{s \leftarrow}^{i \setminus j}(x_i^s)$  for  $s = t, t+1$  are available. The latter quantities are computed by means of time-forward and time-backward update rules from the current set of cavity messages and require  $O(4T)$  operations. In summary, a complete update of the cavity marginals  $m_{i \setminus j}^t$  and cavity fields  $\mu_{i \setminus j}^t$ , for every directed edge and time step, requires  $O(4|E|T)$ .

A Julia-based reference implementation of the above algorithm is available at [28]. Notice that from Eq. (34e),  $\mu_{i \setminus j}^t$  is zero if the time-backward cavity messages at time  $t+1$  are equal. It is shown in Section V A and in Appendix B that this condition is satisfied when no observations are present at later times and it leads to a pure time-forward reduction of the SCDC equations. Furthermore, because of the non-recurrent property of the SI model, it is possible to derive an alternative efficient formulation of the SCDC equations exploiting the infection-time representation: this is explained in detail in Appendix C.

#### IV. GENERALIZATION TO OTHER EPIDEMIC MODELS

The method generalizes directly to models with a higher number of individual states and transitions. In particular, for the Susceptible-Infected-Susceptible (SIS) and Susceptible-Infected-Removed (SIR) models, there is only one additional transition where an infected individual  $i$  can recover at time  $t$  with probability  $r_i^t$ , with the result that the individual  $i$  is either susceptible again (for the SIS model) or in a state of acquired immunity (for the SIR model). A further generalization can be made for the Susceptible-Infected-Removed-Susceptible (SIRS), where each recovered individual  $i$  can return to the susceptible state at time  $t$  due to loss of immunity with probability  $\sigma_i^t$ .

For the SIS model, the only difference with the method described in the previous sections is in the expression of the  $2 \times 2$  transfer matrix, which is now given by

$$M_{x_i^t x_i^{t+1}}^{i \setminus j} = \begin{pmatrix} M_{t,00}^{i \setminus j} & M_{t,01}^{i \setminus j} \\ M_{t,10}^{i \setminus j} & M_{t,11}^{i \setminus j} \end{pmatrix} = \begin{pmatrix} (1 - \varepsilon_i^t) e^{\sum_{k \in \partial i \setminus j} m_{k \setminus i}^t \nu_{ki}^t} p(O_i^t | 0) & \left[1 - (1 - \varepsilon_i^t) e^{\sum_{k \in \partial i \setminus j} m_{k \setminus i}^t \nu_{ki}^t}\right] p(O_i^t | 0) \\ r_i^t e^{\sum_{k \in \partial i \setminus j} \mu_{k \setminus i}^t \nu_{ki}^t} p(O_i^t | 1) & (1 - r_i^t) e^{\sum_{k \in \partial i \setminus j} \nu_{ik}^t \mu_{k \setminus i}^t} p(O_i^t | 1) \end{pmatrix} \quad (35)$$

In the case of the SIR model, each individual  $i$  can be in three possible states  $x_i^t \in \{S, I, R\}$ , but the derivation done for two-state models can be repeated almost straightforwardly (see Appendix D for details). It is still necessary to introduce the marginals  $m_{i \setminus j}^t$  and  $\mu_{i \setminus j}^t$ , defined as follows

$$m_{i \setminus j}^t = \frac{\rho_{\rightarrow t}^{i \setminus j}(I) \rho_{t \leftarrow}^{i \setminus j}(I)}{\sum_{x_i^t} \rho_{\rightarrow t}^{i \setminus j}(x_i^t) \rho_{t \leftarrow}^{i \setminus j}(x_i^t)} \quad (36)$$

$$\mu_{i \setminus j}^t = \frac{\rho_{\rightarrow t}^{i \setminus j}(S) (1 - \varepsilon_i^t) e^{\sum_{k \in \partial i \setminus j} m_{k \setminus i}^t \nu_{ki}^t} p(O_i^t | S) \left( \rho_{t+1 \leftarrow}^{i \setminus j}(S) - \rho_{t+1 \leftarrow}^{i \setminus j}(I) \right)}{\sum_{x_i^t} \rho_{\rightarrow t}^{i \setminus j}(x_i^t) \rho_{t \leftarrow}^{i \setminus j}(x_i^t)}, \quad (37)$$

where the quantities  $\rho_{\rightarrow t}^{i \setminus j}(x_i^t)$  and  $\rho_{t \leftarrow}^{i \setminus j}(x_i^t)$  satisfy a set of equations analogous to (33), with a  $3 \times 3$  matrix  $M_{x_i^t x_i^{t+1}}^{i \setminus j}$  given by

$$M_{x_i^t x_i^{t+1}}^{i \setminus j} = \begin{pmatrix} (1 - \varepsilon_i^t) e^{\sum_{k \in \partial i \setminus j} m_{k \setminus i}^t \nu_{ki}^t} p(O_i^t | S) & \left[1 - (1 - \varepsilon_i^t) e^{\sum_{k \in \partial i \setminus j} m_{k \setminus i}^t \nu_{ki}^t}\right] p(O_i^t | S) & 0 \\ 0 & (1 - r_i^t) e^{\sum_{k \in \partial i \setminus j} \nu_{ik}^t \mu_{k \setminus i}^t} p(O_i^t | I) & r_i^t e^{\sum_{k \in \partial i \setminus j} \nu_{ik}^t \mu_{k \setminus i}^t} p(O_i^t | I) \\ 0 & 0 & p(O_i^t | R) \end{pmatrix}. \quad (38)$$

The SIRS model differs from the SIR model only for the  $3 \times 3$  transfer matrix, which is given by

$$M_{x_i^t x_i^{t+1}}^{i \setminus j} = \begin{pmatrix} (1 - \varepsilon_i^t) e^{\sum_{k \in \partial i \setminus j} m_{k \setminus i}^t \nu_{ki}^t} p(O_i^t | S) & \left[1 - (1 - \varepsilon_i^t) e^{\sum_{k \in \partial i \setminus j} m_{k \setminus i}^t \nu_{ki}^t}\right] p(O_i^t | S) & 0 \\ 0 & (1 - r_i^t) e^{\sum_{k \in \partial i \setminus j} \nu_{ik}^t \mu_{k \setminus i}^t} p(O_i^t | I) & r_i^t e^{\sum_{k \in \partial i \setminus j} \nu_{ik}^t \mu_{k \setminus i}^t} p(O_i^t | I) \\ \sigma_i^t p(O_i^t | R) & 0 & (1 - \sigma_i^t) p(O_i^t | R) \end{pmatrix}. \quad (39)$$

As long as further compartments are included with transitions being parametrized by individual-based rates, generalization of the above construction follows straightforwardly (e.g. SEIR and SEIRS models).

## V. RESULTS

In this Section, we provide numerical results to highlight the operation and capabilities of this method. We first analyze the quality of the approximation for time-forward dynamics obtained in the absence of observations; then we effectively demonstrate the role of the cavity fields  $\mu_{i \setminus j}^t$  in the presence of observations; finally, we evaluate the performances of the SCDC method in various instances of epidemic inference, both on synthetic and real-world contact networks.

### A. Time-forward dynamics

Causality-breaking is a consequence of the existence of observations at later times, that have to be taken into account in the mathematical model by a flux of information flowing backward in time and conditioning the whole history of the process. This property reflects in the existence of non-trivial values for the one-time cavity fields  $\mu_{i \setminus j}^t$ . On the other hand, when no observation is present it is possible to show that all the cavity fields  $\mu_{i \setminus j}^t$  vanish and, consequently, one can recover the usual causal time-forward mean-field dynamics. To prove this, it is convenient to start from a particular form of the update equations for the cavity marginals  $m_{i \setminus j}^t$  (see Appendix B for a derivation),

$$m_{i \setminus j}^t = m_{i \setminus j}^{t-1} + \left(1 - m_{i \setminus j}^{t-1}\right) \frac{\left\{1 - (1 - \varepsilon_i^{t-1}) e^{\sum_{k \in \partial i \setminus j} m_{k \setminus i}^{t-1} \nu_{ki}^{t-1}}\right\} \rho_{t \leftarrow}^{i \setminus j}(1)}{\left(1 - \varepsilon_i^{t-1}\right) e^{\sum_{k \in \partial i \setminus j} m_{k \setminus i}^{t-1} \nu_{ki}^{t-1}} \rho_{t \leftarrow}^{i \setminus j}(0) + \left\{1 - (1 - \varepsilon_i^{t-1}) e^{\sum_{k \in \partial i \setminus j} m_{k \setminus i}^{t-1} \nu_{ki}^{t-1}}\right\} \rho_{t \leftarrow}^{i \setminus j}(1)}, \quad (40)$$

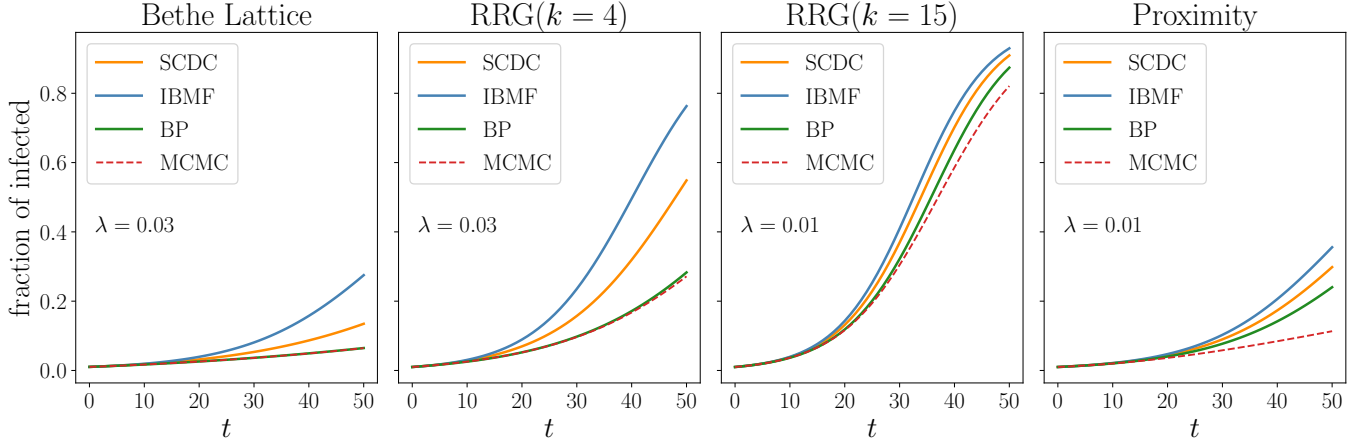


Figure 1. **Forward dynamics with SCDC and other mean field methods.** In each panel, the fraction of infected individuals is shown against the running time of the epidemic, with four different static contact graphs. Comparison is shown between SCDC, IBMF, BP and MonteCarlo simulations (with  $M = 10^4$  samples). All the links have the same infection probability  $\lambda$ , whose value is reported inside each panel. From left to right: Bethe lattice (tree) with degree  $k = 4$  and  $N = 485$ , random regular graph (RRG) with  $N = 500$  and degree  $k = 4$ , RRG with  $N = 500$  and  $k = 15$ , Proximity graph with  $N = 500$  (details about its construction are given in Sec. VC). In all cases, the probability of each individual being infected at time  $t = 0$  is set to  $\gamma^0 = 5/N$ , and the self-infection  $\varepsilon_i^t$  is set to 0.

where the messages  $\rho_{t \leftarrow}^{i \setminus j}(x_i^t)$  represent the (non-normalized) backward probability that state  $x_i^t \in \{0, 1\}$  given the dynamic constraints and the observations in the future. In the absence of observations (on all nodes at all times  $t' \geq t$ ) the backward probability is balanced, i.e.  $\rho_{t \leftarrow}^{i \setminus j}(0) = \rho_{t \leftarrow}^{i \setminus j}(1)$ , and Eq. (40) reduces to time-forward mean-field equations,

$$m_{i \setminus j}^t = m_{i \setminus j}^{t-1} + \left(1 - m_{i \setminus j}^{t-1}\right) \left[1 - (1 - \varepsilon_i^{t-1}) e^{\sum_{k \in \partial i \setminus j} m_k^{t-1} \nu_{ki}^{t-1}}\right], \quad (41)$$

and for the total marginals  $m_i^t$

$$m_i^t = m_i^{t-1} + (1 - m_i^{t-1}) \left[1 - (1 - \varepsilon_i^{t-1}) e^{\sum_{j \in \partial i} m_j^{t-1} \nu_{ji}^{t-1}}\right]. \quad (42)$$

It is possible to verify numerically that, in the absence of observations, the SCDC algorithm in Eqs. (25) and (26) always converges to the same result obtained by running the time-forward Eqs. (41).

An intuitive form for the discrete-time IBMF dynamics, obtained by assuming independence of individual marginal probabilities of being infected, is given by the equations [22, 23],

$$m_i^t = m_i^{t-1} + (1 - m_i^{t-1}) \left[1 - (1 - \varepsilon_i^{t-1}) \prod_{j \in \partial i} (1 - \lambda_{ji}^{t-1} m_j^{t-1})\right]. \quad (43)$$

For a densely-connected graph (for which  $m_{j \setminus i}^t \approx m_j^t$ ) with small infection probabilities ( $\lambda_{ji}^t \ll 1$ ), equations (42) and (43) reduce to the same expression.

Figure 1 illustrates the quality of the approximation obtained using Eqs. (41)-(42) for studying purely time-forward SI dynamics, in the absence of observations. The simulations were performed on well-known classes of static graphs, i.e. contact graphs where two individuals are in contact at all times or at no time. Comparisons are shown between the Small-Coupling Dynamic Cavity method (SCDC), the Belief Propagation (BP) algorithm, and individual-based mean-field equations (IBMF, corresponding to Eqs. (43)). As a reference, the results obtained with numerical sampling from  $10^4$  realizations of the exact time-forward Monte Carlo dynamics of the SI model are also reported. All methods based on mean-field approximations tend to overestimate the number of infected individuals in cases in which the assumed factorization of probabilities is not exact. The BP algorithm is exact on trees (Bethe Lattice) and very accurate on sparse random graphs, where both SCDC and IBMF instead considerably overestimate the number of infected individuals. The performances of all methods are good on dense random graphs and much worse on graphs with spatial structure, such as proximity random graphs (see Sec. VC for details of construction). In all cases under study, the SCDC approximation gives consistently better results than those obtained using IBMF.

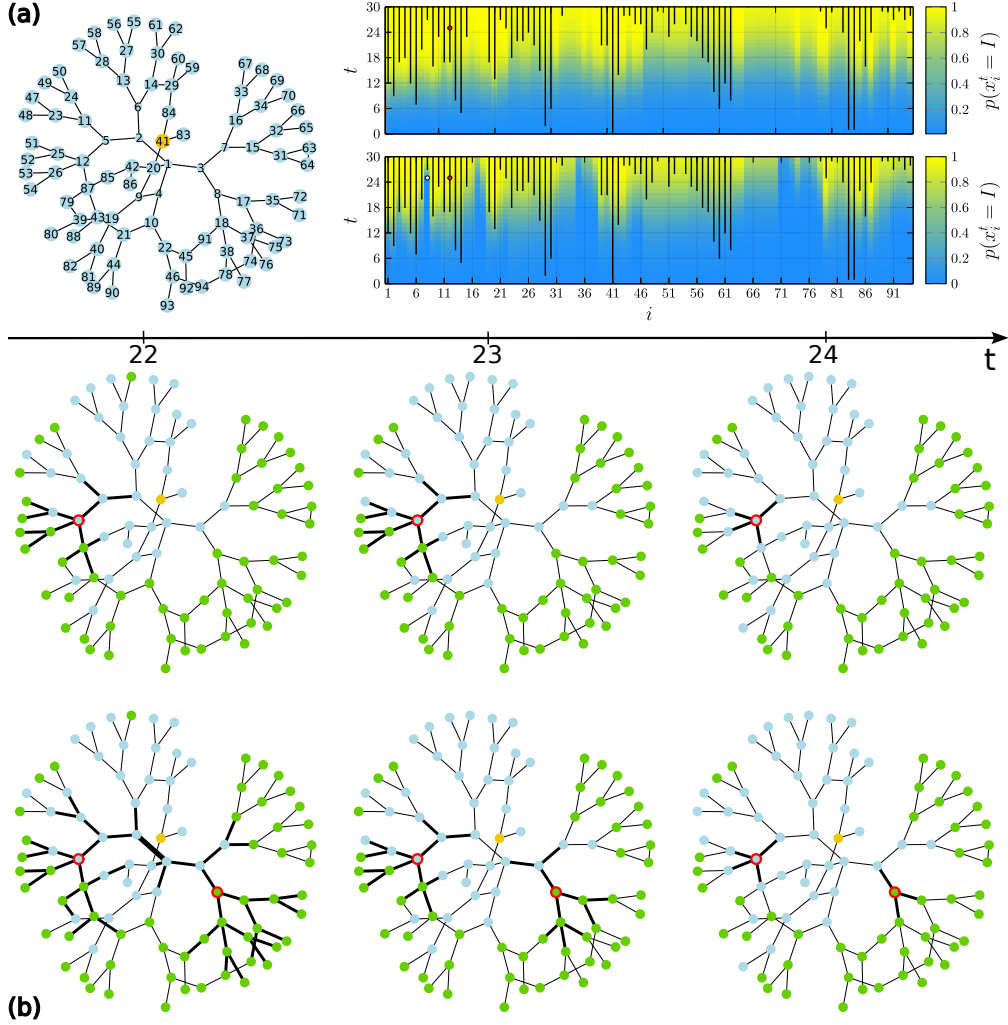


Figure 2. **Behavior of cavity fields  $\mu_{i \setminus j}^t$  in the presence of observations.** Panel (a)-left: contact graph obtained randomly adding links to a tree; the epidemic source is shown as a yellow node. Panel (a)-right: inference performance of SCDC with one observation (top) and two observations (bottom). The two plots show the posterior probability of being infected as a function of time (varying on the  $y$ -axis) for all nodes of the contact graph (a, left) in a single epidemic outbreak generated according to a uniform SI model with  $\lambda = 0.19$ . The same parameter was used to perform the inference. Specifically, the top plot corresponds to one observation on node 12 at time 25, while the bottom one corresponds to two observations on nodes 12 and 8 at time 25. The corresponding state of the observations is represented by colored dots (white = S, red = I, black = R). Black vertical lines mark the true infection periods. (b) Backpropagation through time of the  $\mu$  cavity fields due to observations. The observed individuals are marked by a red circle. Infected individuals are marked by a blue dot, while susceptible individuals are green. The first line of plots corresponds to one observation, while the second line corresponds to two observations. Time flows from left to right, as shown in the time arrow on the top. Thin edges correspond to vanishing  $\mu$  fields, thick edges corresponds to one of the two cavity fields  $\mu_{i \setminus j}^t$  or  $\mu_{j \setminus i}^t$  being non-vanishing, and the thickest edges correspond to both of them being non-vanishing. Observations lead to the activation of  $\mu$  fields, which propagate back in time away from the observed nodes. The portions of the graph where the  $\mu$  messages are non-vanishing have better predictions, meaning that the  $\mu$  fields are fundamental for Bayesian inference.

## B. Effects of backward messages

When at least one observation is included as evidence, the  $\mu$  cavity fields are non-zero and cause a time-backward propagation of information which changes the probabilistic weight of the epidemic trajectories. In order to better understand how the method behaves in the presence of observations, we checked on which edges the absolute value of the  $\mu$  cavity messages is non-vanishing when one or more observations are considered. In particular, we sampled a single epidemic outbreak from a uniform SI model with  $\lambda = 0.19$ , on a contact graph built by randomly adding

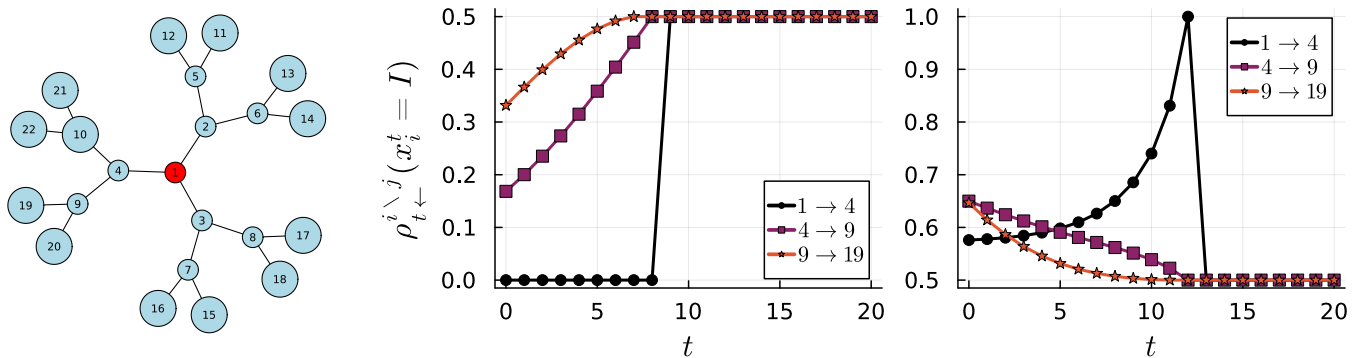


Figure 3. **Time-backward propagation of information generated by observations.** Backward cavity messages  $\rho_{t\leftarrow}^{i\leftarrow j}(x_i^t = I)$  plotted over time for different edges of a small tree. The epidemic outbreak is sampled using a uniform SI model with  $\lambda = 0.1$ . The plot on the left shows the graph. The observed individual is marked red, while the unobserved are blue. The observed node becomes infected at time  $t = 10$ . The plot on the center shows the messages when observing the central node being susceptible at time  $t_o = 8$ . The messages exiting from the observed node suddenly jump from  $\rho_{t\leftarrow}^{i\leftarrow j}(x_i^t = I) = 0$  to  $\rho_{t\leftarrow}^{i\leftarrow j}(x_i^t = I) = 0.5$  at the observation time, while the magnitude of the transition decreases away from the observed node. The plot on the right shows the messages when observing the central node being infected at time  $t_o = 12$ . The messages exiting from the observed node have a sudden jump to  $\rho_{t\leftarrow}^{i\leftarrow j}(x_i^t = I) = 1$ , while the ones exiting from the neighbors of the observed node increase away from the observation time in order to explain the observed infection.

some edges between nodes of a tree. Figure 2 (a) shows how the fields  $\mu_{i\leftarrow j}^t$  propagate into the contact graph up to three times before the observation. For each edge  $(i, j)$  a thick line is plotted if one of the two messages  $\mu_{i\leftarrow j}^t$  or  $\mu_{j\leftarrow i}^t$  is non-vanishing. A thicker line is plotted if both of them are non-vanishing. The plots are shown both for a single observation (top) and two observations (bottom). The plot on the right of Figure 2 (b) shows the inference accuracy of the method for the two cases. We can see that adding an observation greatly increases the performance. In particular, the prediction is improved mostly on the branches of the contact tree where the new observation produces the propagation of the cavity fields  $\mu$ . It is clear that observations lead to the activation of the  $\mu$  fields, which then propagate back in time away from the observed nodes.

A more intuitive probabilistic interpretation of the role of  $\mu$  cavity fields in propagating the information obtained from observations can be obtained by monitoring the temporal behavior of the (normalized) time-forward and time-backward messages  $\rho_{\rightarrow t}^{i\rightarrow j}$  and  $\rho_{t\leftarrow}^{i\leftarrow j}$ . Consider a realization of the SI model taking place on a small tree, as displayed in Figure 3 (left), in which the root node gets infected at time  $t = 10$ . An observation of the state of the root node at a time  $t_o$  introduces a source of information that affects the temporal behavior of the messages  $\rho_{\rightarrow t}^{i\rightarrow j}$  and  $\rho_{t\leftarrow}^{i\leftarrow j}$  for all directed edges  $(i, j)$  at all times. In particular, Figure 3 shows the time-backward messages  $\rho_{t\leftarrow}^{i\leftarrow j}$  as function of time on a set of edges for  $t_o = 8$  (center) and  $t_o = 12$  (right). The observation of a susceptible node (center) implies that at all times before the observation, the message emerging from that node is exactly zero. Moving away from the observed node the time-backward probability is non-zero (and monotonically increasing with the spatial distance) but monotonically decreasing with time distance from the observation. If instead the root node is observed in the infected state, the time-backward message shows an instantaneous jump to 1 at the time of observation and gradually decreases at earlier times, as the time-backward probability of being infected for the root node decreases. Moving away from the root, the messages increase as time proceeds backward indicating that surrounding nodes might have caused the infection of the observed one. Clearly, the (normalized) time-backward messages are exactly equal to 0.5 when no information is available, i.e. at later time steps compared to the observation. Time-forward messages  $\rho_{\rightarrow t}^{i\rightarrow j}$  are not analyzed in detail but they exhibit a similar, though more intuitive, phenomenology.

### C. Inference performance

We consider a typical risk assessment scenario of epidemic inference in which, given the network of contacts and some observations made on an epidemic realization with one initially infected individual, one has to find the probability of each individual being infected at the final time. The simulations of the epidemic realizations according to the SI model are performed using the EpiGen python package [29] on both synthetic and real-world contact networks. The observations are performed on a random subset of the population at the final time. Once the individual probability

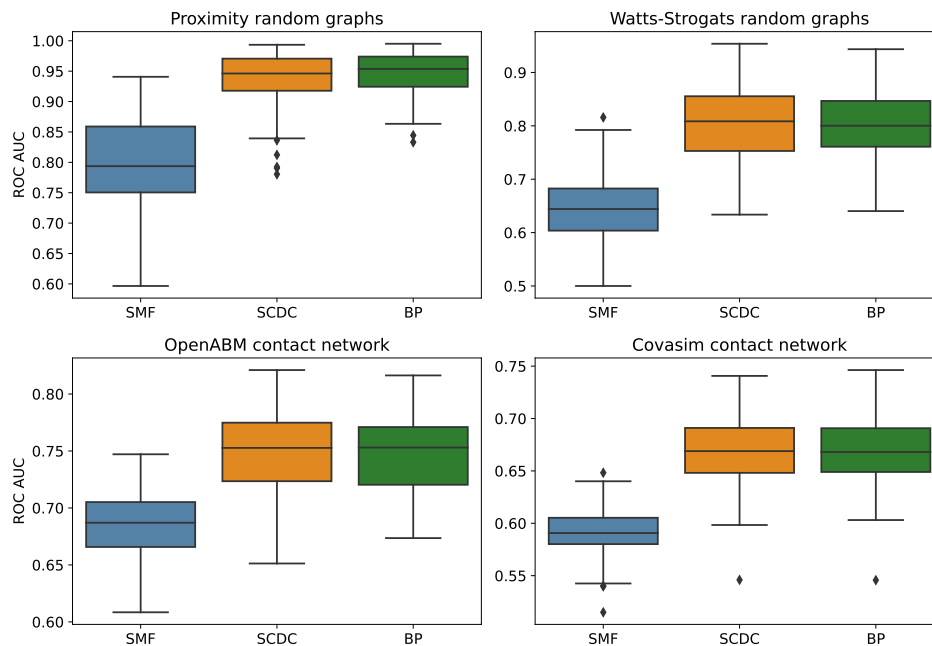


Figure 4. **Epidemic risk assessment of inference methods on random networks.** Epidemic risk assessment on four different classes of random contact networks: soft random geometric graphs (top left), Watts-Strogatz random networks (top right), OpenABM contact network (bottom left) and Covasim contact network (bottom right). The performances of SMF, BP and SCDC are compared in the problem of classifying the infection state of  $N - n_{obs}$  unobserved individuals at the last time  $T$  of SI epidemic processes when a small number  $n_{obs}$  of random observations are provided at the same time  $T$  of the epidemic process. The performance is quantified by computing the area under the curve (AUC) for the Receiver Operating Characteristic (ROC) curves for 100 epidemic realizations for each class of contact network. The boxplots provide summary statistics of performances, in which whiskers extend at most to 1.5 times the inter-quartile range, or to the maximum (resp. minimum) value if lower (resp. higher). Diamonds represent outliers. Other parameters: soft random geometric graphs ( $N = 600$ ,  $l_{max} = \sqrt{2.8/N}$ ,  $n_{obs} = 20$ ,  $T = 28$ ,  $\lambda = 0.08$ ), Watts-Strogatz graphs ( $N = 600$ , average degree  $z = 4$ ,  $p_{rw} = 0.12$ ,  $n_{obs} = 20$ ,  $T = 25$ ,  $\lambda = 0.16$ ), OpenABM ( $N = 2000$ ,  $n_{obs} = 60$ ,  $T = 21$ ,  $\gamma = 0.026$ ) and Covasim ( $N = 1000$ ,  $n_{obs} = 40$ ,  $T = 24$ ,  $\gamma = 0.038$ ).

of being infected at the final time is estimated with an epidemic inference method, the knowledge of the ground truth provided by the corresponding epidemic realization allows to compute a ROC curve of true infected individuals vs. false infected individuals. The area under the ROC curve (AUC) represents an estimate of the probability of correct classification of the individual infection states. The inference through SCDC is carried out using the infection-time representation (discussed in Appendix C), and its performances are evaluated in comparison with two well-established methods for distributed epidemic inference, the Simple Mean Field (SMF) method [2] and the Belief Propagation (BP) algorithm [2, 13]. For both BP and SCDC methods, the individual probability of being infected at the final time is computed from the corresponding total marginals once the message passing algorithm has reached convergence, i.e. the error on the cavity marginals decreases under a predefined tolerance threshold. In some cases, BP and SCDC do not reach convergence in a reasonable number of iterations (a few thousand in the case of the epidemic instances under study). The lack of convergence can be due to a relevant role played by loop structures and long-range correlations. In such cases, the probability marginals are computed taking an average over a sufficiently large number (up to hundreds) of iterations of the message passing update. The Simple Mean Field (SMF) inference method introduced in [2] is instead an inference method based on the IBMF approximation for the SI dynamics in which the information provided by observations of susceptible and infected individuals is taken into account by introducing some specific constraints on the time-forward dynamics (see Ref.[2] for a description in the more general SIR model).

In Figure 4 the results for different kinds of synthetic contact graphs are shown. The top panels show results for two classes of static random graphs: Watts-Strogatz graphs [30], and soft random geometric graphs [31]. In the Watts-Strogatz model, the edges of a pristine network with a regular locally connected structure are rewired randomly with a probability  $p_{rw}$ , leading to the emergence of non-trivial small-world and clustering properties. In soft random geometric graphs, also known as proximity random graphs, individuals are distributed uniformly at random in the unit square, then only pairs at Euclidean distance  $l < l_{max}$  are connected with a probability which decays exponentially



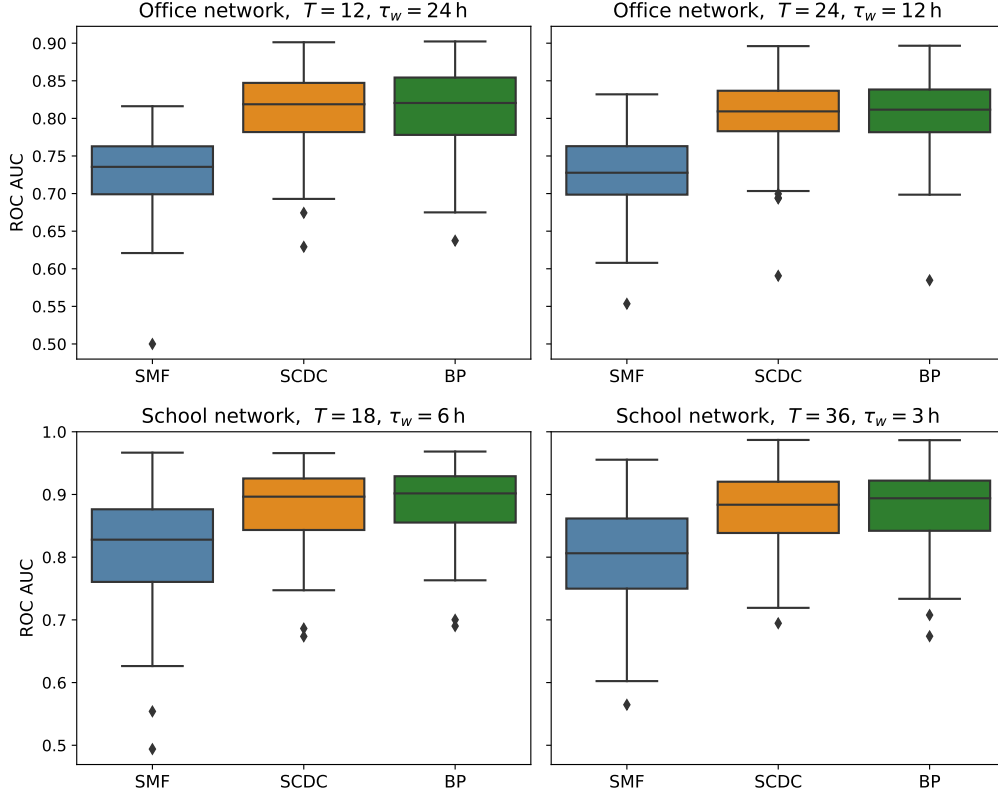


Figure 5. **Epidemic risk assessment of inference methods on real-world contact networks.** Epidemic inference on two real contact networks: office network from the InVS15 dataset (top panels) and school network from the Thiers13 dataset (bottom panels). Two different sizes  $t_w$  of time windows were used to aggregate contact data. The performances of SMF, BP and SCDC are compared in the problem of classifying the infection state of  $N - n_{obs}$  unobserved individuals at the last time  $T$  of SI epidemic processes when a small number  $n_{obs}$  of random observations are provided at the last time of the epidemic process. The performance is quantified by computing the area under the curve (AUC) for the Receiver Operating Characteristic (ROC) curves for 100 epidemic realizations for each class of contact network. The boxplots provide summary statistics of performances, in which whiskers extend at most to 1.5 times the inter-quartile range, or to the maximum (resp. minimum) value if lower (resp. higher). Diamonds represent outliers. Other parameters: office network ( $N = 219$ ,  $n_{obs} = 15$ ,  $t_w = 24\text{h}$ ,  $T = 12$  and  $t_w = 12\text{h}$ ,  $T = 24$ ,  $\gamma = 6 \cdot 10^{-4}$ ), school network ( $N = 328$ ,  $n_{obs} = 20$ ,  $t_w = 6\text{h}$ ,  $T = 18$  and  $t_w = 3\text{h}$ ,  $T = 36$ ,  $\gamma = 7 \cdot 10^{-5}$ ).

with  $l$ . Both classes of random networks are locally highly structured, with short loops and clusters. The bottom panels refer to synthetic contact networks generated with more realistic agent-based models, the OpenABM-Covid19 [32] and Covasim [33] models. These agent-based models are able to generate realistic contact networks on large populations, by modeling the interactions in households, schools, workplaces and other locations. Some contacts in these networks also change daily to reflect the dynamic nature of real-life interactions. Only the contact network structures generated by these agent-based models over a time horizon of a few weeks is used in the present work, and the epidemic propagations are generated using the standard SI model. In these networks, the link between two individuals  $i$  and  $j$  is assigned a weight  $w_{ij}^t$ , representing the aggregate duration of the contact between  $i$  and  $j$  in day  $t$ . Given an infection rate  $\gamma$  per contact per time unit, the infection probability associated to the contact is then computed as  $\lambda_{ij}^t = 1 - e^{-\gamma w_{ij}^t}$ . In both cases, when a relatively small number of observations is provided at the last time, the SCDC method is able to outperform SMF and achieves accuracy on par with the BP method.

The same testing framework is also employed to evaluate epidemic inference on two real contact networks, originally presented in Ref. [34], that have been collected with RFID tags in a school (Thiers13 dataset) and in an office environment (InVS15 datasets). The contact data are collected over a period of several days, with a temporal resolution of 20 seconds, which allows for data aggregation over coarse-grained time windows of a preferred size  $\tau_w$ . In our study, time windows with size  $\tau_w$  ranging from 3 hours to a day are considered, for a total of  $T$  time steps ranging from a minimum of 12 to a maximum of 36 steps. When performing the coarse-graining procedure, the number  $c_{ij}^t$  of contacts between  $i$  and  $j$  occurring in a time window  $t$  of size  $\tau_w$  is computed and used to estimate the infection



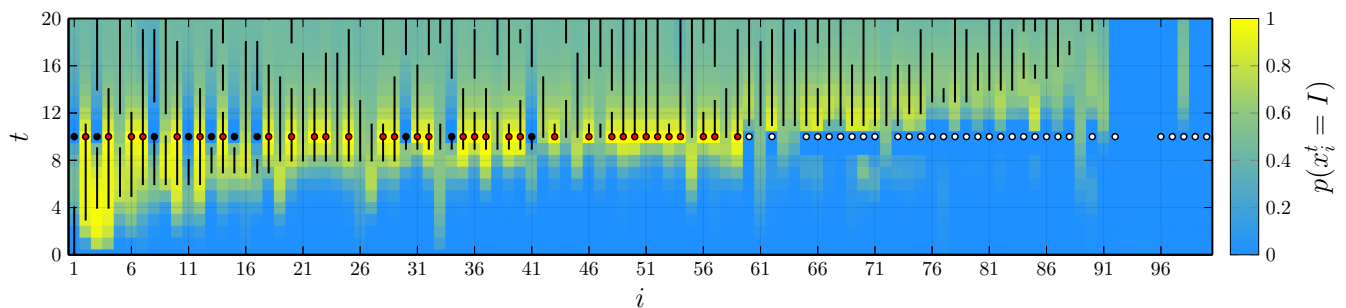


Figure 6. **Inference in recurrent epidemic models.** Posterior probability of being infected as a function of time for all nodes of an Erdos-Renyi random graph ( $N = 100$  nodes and average degree  $z = 3$ ) in a single epidemic outbreak generated according to a uniform SIRS model. The parameters of the SIRS model are  $\lambda = 0.4$ ,  $r = \sigma = 0.15$ , for all nodes at all times. The same parameters were used to perform the inference. The 75% of the nodes were randomly observed at the same time 10, and their corresponding state is represented by colored dots (white=S, red=I, black=R). Black vertical lines mark to true infection periods. Node order from left to right reproduces the order of true infection events.

probability  $\lambda_{ij}^t$  between the two individuals at time step  $t$  as  $\lambda_{ij}^t = 1 - (1 - \gamma)^{c_{ij}^t}$ , where  $\gamma$  is a common parameter describing the infectiousness of a single contact. The results of epidemic risk assessment on these real-world contact networks are shown in Figure 5, adopting the same metric used in the case of random graphs. Also in this case, for all contact networks under study, the SCDC method has a performance very close to the BP algorithm, and in general superior to the SMF heuristic.

#### D. Inference in recurrent epidemic models

While previous results focus on the quantitative analysis of inference performances on irreversible dynamics, the present subsection aims at illustrating the potential of the SCDC method for epidemic inference on recurrent epidemic models. In order to do that, we perform a simple analysis inspired by the one already presented in recent work on Matrix Product Belief Propagation [35], a novel powerful approximation method for recurrent dynamics on graphs. We conducted simulations of a single epidemic outbreak using a SIRS model on an Erdos-Renyi random graph with  $N = 100$  nodes and average degree  $z = 3$ . Figure 6 shows the value of the posterior marginal probability of being infected  $p(x_i^t = 0 | \mathcal{O})$  inferred by the SCDC method. The color scale indicating these probability values is superimposed on the black bars marking the time intervals of true infections, which enables visual inspection of the inference performance of the method. Notably, the SCDC method rather accurately assigns posterior marginal probabilities that closely align with the observed data, demonstrating its effectiveness even for unobserved nodes or time points that are distant from the observations. Several reinfection events are also correctly captured. Although the preliminary results are promising, further investigations are needed to fully understand the performance of the SCDC method on inference problems involving recurrent epidemic models. However, conducting these additional investigations is outside the scope of the current study.

## VI. CONCLUSIONS

The Dynamic Cavity method is a distributed technique to study discrete-state stochastic processes on graphs, which is exact on trees and often provides very good approximations on sparse graphs. While its original formulation is computationally demanding [16, 17], approximations have been introduced [36–41] and, whenever possible, more efficient parameterizations of single dynamical trajectories have been introduced [12, 13, 19]. In the present work, an observation-reweighted version of the Dynamic Cavity formulation, including individual observations, is introduced to model the posterior probability of epidemic processes on contact networks. The formulation exploits a Bayesian approach and is fully equivalent to the Belief Propagation approach to epidemic trajectories [12, 13]. Starting from the reweighted Dynamic Cavity formulation and exploiting a small-coupling expansion, a novel set of fixed-point equations for a pair of time-dependent cavity messages  $m_{i \setminus j}^t$  and  $\mu_{i \setminus j}^t$  is obtained. Here,  $m_{i \setminus j}^t$  is the probability that individual  $i$  is infected at time  $t$  in the cavity graph when the interaction with individual  $j$  is removed, while  $\mu_{i \setminus j}^t$  is a

cavity field whose role depends on the presence of observations. In the absence of observations, all cavity fields  $\{\mu_{i \setminus j}^t\}$  identically vanish, and the dynamics, expressed solely in terms of marginal probabilities  $\{m_{i \setminus j}^t\}$ , becomes causal, reducing to a set of generalized mean-field equations. These time-forward equations, tested on random graphs for the SI model, yield higher accuracy compared to the commonly used individual-based mean-field equations (which they reduce to in the regime of low infectiousness and high connectivity), albeit less accurate than BP, which in the simplified case of non-recurrent forward dynamics coincides with the Dynamic Message Passing method [18, 19]. Simple analyses conducted on the SI model with limited observations demonstrate that the role of the cavity fields  $\{\mu_{i \setminus j}^t\}$  is to propagate information about observations to neighboring nodes and subsequently distribute this information throughout the contact network, appropriately tilting the probabilistic weight of the associated dynamic trajectories in view of the presence of observations. The presence of observations renders the epidemic dynamics non-causal, with backward-in-time information flow, as evident from the non-uniform distribution of the backward cavity messages  $\rho_{i \leftarrow}^{i \setminus j}(x_i^t)$ . The main additional approximation assumed in deriving the SCDC method from the DC equations is the independence of cavity messages from the epidemic trajectory of the removed node. This approximation can introduce inconsistencies with specific trajectories imposed by observations, particularly in regimes with numerous observations, including repeated observations on the same individuals. However, this issue is effectively resolved by introducing a small self-infection probability, which practically eliminated the problem in all applications considered. The SCDC algorithm proves to be highly effective in assessing the epidemic risk of individuals, exhibiting performance very similar to that of BP, of which it is essentially an approximation, and substantially outperforming other heuristic methods based on mean-field approximations. As a fixed-point message passing method, a potential drawback of SCDC lies in its convergence properties. In numerical tests, SCDC experiences convergence problems similar to BP, mainly resulting from long-range correlations generated by loops in the contact graphs. Nevertheless, even in the absence of convergence, the estimated marginal probabilities often remain sufficiently accurate, enabling a reliable estimation of the epidemic risk.

The main advantage of the SCDC method over Dynamic Cavity and Belief Propagation for epidemic trajectories lies in its straightforward generalization to epidemic models with multiple states (e.g., SIR, SEIR) and recurrent processes (e.g., SIS, SIRS). Indeed, the fundamental components of the method and the efficient algorithm based on the temporal transfer matrix remain largely unchanged, with only modifications in the matrix dimensions and elements to accommodate the model's increased complexity. Consequently, the SCDC algorithm maintains a linear complexity with respect to the duration of the epidemic process and the number of contacts in the network. Preliminary results indicate excellent predictive power even for complex recurrent epidemic processes like the SIRS model. Surprisingly, no assumption of small infectiousness was made in the applications, suggesting that the method performs well beyond the limitations expected from its derivation.

The primary limitation of the SCDC method is that its efficient formulation based on the transfer matrix is currently applicable only to Markovian models. Further study is required to develop an efficient algorithm for non-Markovian recurrent epidemic models. Concerning the method itself, another interesting direction for its development involves gaining a better understanding of the role of second-order terms in the small coupling expansion and developing an improved algorithm that takes them into account. Finally, future directions include the possibility to generalize the approach presented here to other type of dynamical processes on networks, e.g. rumor spreading processes [42, 43].

## VII. ACKNOWLEDGMENTS

Computational resources were provided by the SmartData@PoliTO ([smartdata.polito.it](http://smartdata.polito.it)) interdepartmental center on Big Data and Data Science. We thank S. Crotti for suggesting the format of Figures 2 and 6, similar to what used in Ref. [35]. G.C. acknowledges support by the Comunidad de Madrid and the Complutense University of Madrid (UCM) through the Atracción de Talento programs (Refs. 2019-T1/TIC-13298).

- 
- [1] L. Ferretti, C. Wymant, M. Kendall, L. Zhao, A. Nurtay, L. Abeler-Dörner, M. Parker, D. Bonsall, and C. Fraser, *Science* **368**, eabb6936 (2020).
  - [2] A. Baker, I. Biazzo, A. Braunstein, G. Catania, L. Dall'Asta, A. Ingrosso, F. Krzakala, F. Mazza, M. Mézard, A. P. Muntoni, M. Refinetti, S. S. Mannelli, and L. Zdeborová, *Proceedings of the National Academy of Sciences* **118**, e2106548118 (2021).
  - [3] D. Shah and T. Zaman, *SIGMETRICS Perform. Eval. Rev.* **38**, 203–214 (2010).
  - [4] D. Shah and T. Zaman, *IEEE Transactions on information theory* **57**, 5163 (2011).
  - [5] A. Y. Lokhov, M. Mézard, H. Ohta, and L. Zdeborová, *Physical Review E* **90**, 012801 (2014).
  - [6] N. Antulov-Fantulin, A. Lančić, T. Šmuc, H. Štefančić, and M. Šikić, *Physical review letters* **114**, 248701 (2015).

- [7] I. Biazzo, A. Braunstein, L. Dall'Asta, and F. Mazza, *Scientific Reports* **12**, 19673 (2022).
- [8] A. Braunstein, G. Catania, L. Dall'Asta, M. Mariani, and A. P. Muntoni, *Scientific Reports* **13**, 7350 (2023), number: 1 Publisher: Nature Publishing Group.
- [9] C. Shah, N. Dehmamy, N. Perra, M. Chinazzi, A.-L. Barabási, A. Vespignani, and R. Yu, arXiv preprint arXiv:2006.11913 [10.48550/arXiv.2006.11913](https://arxiv.org/abs/2006.11913) (2020).
- [10] S. Chen, P.-D. Yu, C. W. Tan, and H. V. Poor, arXiv preprint arXiv:2211.00880 [10.48550/arXiv.2211.00880](https://arxiv.org/abs/2211.00880) (2022).
- [11] G. Čutura, B. Li, A. Swami, and S. Segarra, in [2021 29th European Signal Processing Conference \(EUSIPCO\)](https://doi.org/10.1109/EUSIPCO45924.2021) (2021) pp. 2204–2208.
- [12] F. Altarelli, A. Braunstein, L. Dall'Asta, A. Lage-Castellanos, and R. Zecchina, *Physical review letters* **112**, 118701 (2014).
- [13] F. Altarelli, A. Braunstein, L. Dall'Asta, A. Ingrosso, and R. Zecchina, *Journal of Statistical Mechanics: Theory and Experiment* **2014**, P10016 (2014).
- [14] A. Braunstein and A. Ingrosso, *Scientific reports* **6**, 1 (2016).
- [15] J. Bindi, A. Braunstein, and L. Dall'Asta, *Plos one* **12**, e0176376 (2017).
- [16] I. Neri and D. Bollé, *Journal of Statistical Mechanics: Theory and Experiment* **2009**, P08009 (2009).
- [17] Y. Kanoria and A. Montanari, *The Annals of Applied Probability* **21**, 1694 (2011).
- [18] A. Y. Lokhov, M. Mézard, and L. Zdeborová, *Physical Review E* **91**, 012811 (2015).
- [19] F. Altarelli, A. Braunstein, L. Dall'Asta, and R. Zecchina, *Physical Review E* **87**, 062115 (2013).
- [20] S. Gómez, A. Arenas, J. Borge-Holthoefer, S. Meloni, and Y. Moreno, *Europhysics Letters* **89**, 38009 (2010).
- [21] P. Van Mieghem, J. Omic, and R. Kooij, *IEEE/ACM Transactions On Networking* **17**, 1 (2008).
- [22] I. Z. Kiss, J. C. Miller, and P. L. Simon, [Mathematics of Epidemics on Networks: From Exact to Approximate Models](https://doi.org/10.1007/978-1-4939-9832-7_46), Interdisciplinary Applied Mathematics, Vol. 46 (Springer International Publishing, 2017).
- [23] R. Pastor-Satorras, C. Castellano, P. Van Mieghem, and A. Vespignani, *Reviews of modern physics* **87**, 925 (2015).
- [24] T. Plefka, *Journal of Physics A: Mathematical and General* **15**, 1971 (1982).
- [25] B. Bravi, P. Sollich, and M. Opper, *Journal of Physics A: Mathematical and Theoretical* **49**, 194003 (2016).
- [26] A. Georges and J. S. Yedidia, *Journal of Physics A: Mathematical and General* **24**, 2173 (1991).
- [27] A. Maillard, L. Foini, A. L. Castellanos, F. Krzakala, M. Mézard, and L. Zdeborová, *Journal of Statistical Mechanics: Theory and Experiment* **2019**, 113301 (2019).
- [28] <https://github.com/Mattiatarabolo/SmallCouplingDynamicCavity.jl>.
- [29] F. Mazza and I. Biazzo, *EpiGen: generator of epidemics on contact graphs* (2023).
- [30] D. J. Watts and S. H. Strogatz, *Nature* **393**, 440 (1998).
- [31] M. D. Penrose, *The Annals of Applied Probability* **26**, 986 (2016).
- [32] R. Hinch, W. J. M. Probert, A. Nurtay, M. Kendall, C. Wymant, M. Hall, K. Lythgoe, A. B. Cruz, L. Zhao, A. Stewart, L. Ferretti, D. Montero, J. Warren, N. Mather, M. Abueg, N. Wu, O. Legat, K. Bentley, T. Mead, K. Van-Vuuren, D. Feldner-Busztin, T. Ristori, A. Finkelstein, D. G. Bonsall, L. Abeler-Dörner, and C. Fraser, *PLOS Computational Biology* **17**, e1009146 (2021).
- [33] C. C. Kerr, R. M. Stuart, D. Mistry, R. G. Abeysuriya, K. Rosenfeld, G. R. Hart, R. C. Núñez, J. A. Cohen, P. Selvaraj, B. Hagedorn, L. George, M. Jastrzębski, A. S. Izzo, G. Fowler, A. Palmer, D. Delpont, N. Scott, S. L. Kelly, C. S. Bennette, B. G. Wagner, S. T. Chang, A. P. Oron, E. A. Wenger, J. Panovska-Griffiths, M. Famulare, and D. J. Klein, *PLOS Computational Biology* **17**, e1009149 (2021).
- [34] M. Génois and A. Barrat, *EPJ Data Science* **7**, 11 (2018).
- [35] S. Crotti and A. Braunstein, *Large deviations in stochastic dynamics over graphs through matrix product belief propagation* (2023), [arXiv:2303.17403 \[cond-mat.stat-mech\]](https://arxiv.org/abs/2303.17403).
- [36] E. Aurell and H. Mahmoudi, *Journal of Statistical Mechanics: Theory and Experiment* **2011**, P04014 (2011).
- [37] E. Aurell and H. Mahmoudi, *Physical Review E* **85**, 031119 (2012).
- [38] G. Del Ferraro and E. Aurell, *Physical Review E* **92**, 010102 (2015).
- [39] E. Aurell, G. Del Ferraro, E. Domínguez, and R. Mulet, *Physical Review E* **95**, 052119 (2017).
- [40] E. D. Vázquez, G. Del Ferraro, and F. Ricci-Tersenghi, *Journal of Statistical Mechanics: Theory and Experiment* **2017**, 033303 (2017).
- [41] E. Ortega, D. Machado, and A. Lage-Castellanos, *Physical Review E* **105**, 024308 (2022).
- [42] D. J. Daley and D. G. Kendall, *Nature* **204**, 1118 (1964).
- [43] S. Boccaletti, V. Latora, Y. Moreno, M. Chavez, and D.-U. Hwang, *Physics Reports* **424**, 175 (2006).

### Appendix A: Derivation of the dynamic cavity equations for the SI model

In this Section, a derivation of the dynamic cavity equations (11) is presented. For clarity of exposition, the calculations are carried out for the case of pure time-forward dynamics; the addition of observations is discussed afterward. The derivation exploits a path-integral representation of the stochastic epidemic dynamics of the SI model, that is based on interpreting the (Markovian) update rule of the discrete-time stochastic process as a set of dynamical constraints for the degrees of freedom under study, i.e. the binary variables  $\{x_i^t\}$ , and on defining a dynamic partition function of the form

$$\mathcal{Z} = \sum_{\mathbf{X}} p(\mathbf{X}) \quad (\text{A1a})$$

$$= \sum_{\mathbf{X}} \prod_{i=1}^N \left\{ p(x_i^0) \prod_{t=0}^{T-1} \left[ \sum_{y_i^t, h_i^t} P[y_i^t | h_i^t] \delta_{x_i^{t+1}, x_i^t + (1-x_i^t)y_i^t} \delta \left( h_i^t - \sum_{j=1}^N \nu_{ji}^t x_j^t \right) \right] \right\} \quad (\text{A1b})$$

$$= \sum_{\mathbf{X}, \mathbf{Y}} \int d\mathbf{H} P[\mathbf{Y} | \mathbf{H}] \prod_{i=1}^N \left\{ p(x_i^0) \prod_{t=0}^{T-1} \left[ \delta_{x_i^{t+1}, x_i^t + (1-x_i^t)y_i^t} \delta \left( h_i^t - \sum_{j=1}^N \nu_{ji}^t x_j^t \right) \right] \right\} \quad (\text{A1c})$$

where  $P[\mathbf{Y} | \mathbf{H}] = \prod_{i=1}^N \prod_{t=0}^{T-1} \sum_{y_i^t, h_i^t} P[y_i^t | h_i^t]$  and the time-dependent matrix  $\{\nu_{ij}^t\}$  already defined in Sec. III A encodes the infection rates and possible interaction patterns over time. Using the integral representation of Dirac's and Kronecker's delta functions and replacing the explicit expression of the conditional probabilities  $P[y_i^t | h_i^t]$  from Eq. (5), we obtain

$$\mathcal{Z} = \sum_{\mathbf{X}, \mathbf{Y}} \int d\mathbf{H} P[\mathbf{Y} | \mathbf{H}] \prod_{i=1}^N \left\{ p(x_i^0) \prod_{t=0}^{T-1} \left[ \delta_{x_i^{t+1}, x_i^t + (1-x_i^t)y_i^t} \delta \left( h_i^t - \sum_{j=1}^N \nu_{ji}^t x_j^t \right) \right] \right\} \quad (\text{A2a})$$

$$= \sum_{\mathbf{X}} \prod_{i=1}^N \left\{ p(x_i^0) \prod_{t=0}^{T-1} \left[ \sum_{y_i^t=0,1} \int_{-\infty}^{+\infty} dh_i^t \int_0^{2\pi} \frac{d\hat{x}_i^t}{2\pi} e^{i\hat{x}_i^t(x_i^{t+1} - x_i^t - (1-x_i^t)y_i^t)} [1 - e^{h_i^t(1-\varepsilon_i^t)}]^{y_i^t} [e^{h_i^t(1-\varepsilon_i^t)}]^{(1-y_i^t)} \right. \right. \\ \left. \left. \times \int_{-\infty}^{+\infty} \frac{d\hat{h}_i^t}{2\pi} e^{i\hat{h}_i^t(h_i^t - \sum_{j=1}^N \nu_{ji}^t x_j^t)} \right] \right\} \quad (\text{A2b})$$

$$= \sum_{\mathbf{X}} \prod_{i=1}^N \left\{ p(x_i^0) \prod_{t=0}^{T-1} \left[ \sum_{y_i^t=0,1} \int_{-\infty}^{+\infty} dh_i^t \int_0^{2\pi} \frac{d\hat{x}_i^t}{2\pi} e^{i\hat{x}_i^t(x_i^{t+1} - x_i^t)} e^{-i\hat{x}_i^t(1-x_i^t)y_i^t} [1 - e^{h_i^t(1-\varepsilon_i^t)}]^{y_i^t} [e^{h_i^t(1-\varepsilon_i^t)}]^{(1-y_i^t)} \right. \right. \\ \left. \left. \times \int_{-\infty}^{+\infty} \frac{d\hat{h}_i^t}{2\pi} e^{i\hat{h}_i^t(h_i^t - \sum_{j=1}^N \nu_{ji}^t x_j^t)} \right] \right\}. \quad (\text{A2c})$$

It is convenient to proceed isolating the interaction terms and performing the sums over the random variables  $y_i^t$ ,

$$\mathcal{Z} = \sum_{\mathbf{X}} \prod_{i=1}^N \left\{ p(x_i^0) \prod_{t=0}^{T-1} \left[ \int_{-\infty}^{+\infty} \frac{d\hat{h}_i^t}{2\pi} \int_{-\infty}^{+\infty} dh_i^t e^{i\hat{h}_i^t h_i^t} \int_0^{2\pi} \frac{d\hat{x}_i^t}{2\pi} e^{i\hat{x}_i^t(x_i^{t+1} - x_i^t)} \right. \right. \\ \left. \left. \times \sum_{y_i^t=0,1} e^{-i\hat{x}_i^t(1-x_i^t)y_i^t} [1 - e^{h_i^t(1-\varepsilon_i^t)}]^{y_i^t} [e^{h_i^t(1-\varepsilon_i^t)}]^{(1-y_i^t)} \prod_{j>i} e^{-i(\hat{h}_i^t \nu_{ji}^t x_j^t + \hat{h}_j^t \nu_{ij}^t x_i^t)} \right] \right\} \quad (\text{A3a})$$

$$= \sum_{\mathbf{X}} \prod_{i=1}^N \left\{ p(x_i^0) \prod_{t=0}^{T-1} \left[ \int_{-\infty}^{+\infty} d\hat{h}_i^t \int_0^{2\pi} \frac{d\hat{x}_i^t}{2\pi} e^{i\hat{x}_i^t(x_i^{t+1} - x_i^t)} \int_{-\infty}^{+\infty} \frac{dh_i^t}{2\pi} e^{i\hat{h}_i^t h_i^t} \left[ (1 - e^{h_i^t(1-\varepsilon_i^t)}) e^{-i\hat{x}_i^t(x_i^{t+1} - 1)} + e^{h_i^t(1-\varepsilon_i^t)} \right] \right. \right. \\ \left. \left. \times \prod_{j>i} e^{-i(\hat{h}_i^t \nu_{ji}^t x_j^t + \hat{h}_j^t \nu_{ij}^t x_i^t)} \right] \right\} \quad (\text{A3b})$$

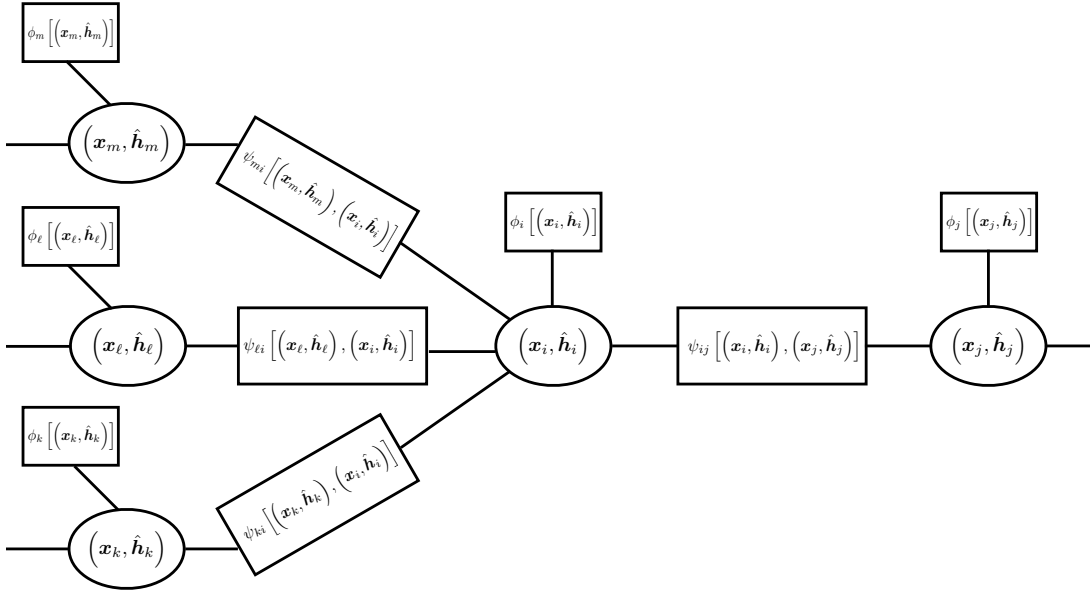


Figure 7. Factor Graph for the graphical model interpretation of the dynamical partition function in Eq. (A4) with factors as given in Eqs. (A5)-(A6).

then performing the integrals over  $h_i^t$  and  $\hat{x}_i^t$ , we get

$$\mathcal{Z} = \sum_{\mathbf{X}} \prod_{i=1}^N \left\{ p(x_i^0) \prod_{t=0}^{T-1} \left[ \int_{-\infty}^{+\infty} d\hat{h}_i^t \int_0^{2\pi} \frac{d\hat{x}_i^t}{2\pi} \left[ \delta(\hat{h}_i^t - i) (1 - \varepsilon_i^t) \left( e^{i\hat{x}_i^t(x_i^{t+1} - x_i^t)} - e^{i\hat{x}_i^t(x_i^{t+1} - 1)} \right) + \delta(\hat{h}_i^t) e^{i\hat{x}_i^t(x_i^{t+1} - 1)} \right] \right. \right. \\ \left. \left. \times \prod_{j>i} e^{-i(\hat{h}_i^t \nu_{ji}^t x_j^t + \hat{h}_j^t \nu_{ij}^t x_i^t)} \right] \right\} \quad (\text{A4a})$$

$$= \sum_{\mathbf{X}} \prod_{i=1}^N \left\{ p(x_i^0) \prod_{t=0}^{T-1} \left[ \int_{-\infty}^{+\infty} d\hat{h}_i^t \left[ \delta(\hat{h}_i^t - i) (1 - \varepsilon_i^t) \left( \delta_{x_i^{t+1}, x_i^t} - \delta_{x_i^{t+1}, 1} \right) + \delta(\hat{h}_i^t) \delta_{x_i^{t+1}, 1} \right] \right. \right. \\ \left. \left. \times \prod_{j>i} e^{-i(\hat{h}_i^t \nu_{ji}^t x_j^t + \hat{h}_j^t \nu_{ij}^t x_i^t)} \right] \right\} \quad (\text{A4b})$$

$$= \sum_{\mathbf{X}} \int D\hat{\mathbf{H}} \prod_{i=1}^N \left\{ p(x_i^0) \prod_{t=0}^{T-1} \left[ \left[ \delta(\hat{h}_i^t - i) (1 - \varepsilon_i^t) \left( \delta_{x_i^{t+1}, x_i^t} - \delta_{x_i^{t+1}, 1} \right) + \delta(\hat{h}_i^t) \delta_{x_i^{t+1}, 1} \right] \right. \right. \\ \left. \left. \times \prod_{j>i} e^{-i(\hat{h}_i^t \nu_{ji}^t x_j^t + \hat{h}_j^t \nu_{ij}^t x_i^t)} \right] \right\} \quad (\text{A4c})$$

where  $\int D\hat{\mathbf{H}} = \prod_{i=1}^N \prod_{t=0}^{T-1} \left( \int_{-\infty}^{+\infty} d\hat{h}_i^t \right)$  for shortness of notation.

The probabilistic weight associated with the dynamic partition function  $\mathcal{Z}$  is now in a form that can be represented as a graphical model, in which the variable nodes correspond to the spatio-temporal variables  $\mathbf{x}_i$  and  $\hat{\mathbf{h}}_i$  and there are two types of factor nodes (see Figure 7): single-node factors

$$\phi_i[(\mathbf{x}_i, \hat{\mathbf{h}}_i)] = p(x_i^0) \prod_{t=0}^{T-1} \left[ \delta(\hat{h}_i^t - i) (1 - \varepsilon_i^t) \left( \delta_{x_i^{t+1}, x_i^t} - \delta_{x_i^{t+1}, 1} \right) + \delta(\hat{h}_i^t) \delta_{x_i^{t+1}, 1} \right] \quad (\text{A5})$$

and factors involving pairs of variables on neighboring nodes at the same time

$$\psi_{ij} \left[ (\mathbf{x}_i, \hat{\mathbf{h}}_i), (\mathbf{x}_j, \hat{\mathbf{h}}_j) \right] = \prod_{t=0}^{T-1} e^{-i(\hat{h}_i^t \nu_{ji}^t x_j^t + \hat{h}_j^t \nu_{ij}^t x_i^t)}. \quad (\text{A6})$$

By grouping together single-node variables at all times, that is trajectories  $(\mathbf{x}_i, \hat{\mathbf{h}}_i) = (\{x_i^0, \dots, x_i^T\}, \{\hat{h}_i^0, \dots, \hat{h}_i^T\})$ , the resulting factor graph reproduces the topology of the underlying interaction graph. It should be noted that the choice of variable grouping in this approach disentangles the locally-loopy structure of the factor graph associated with the space-time problem. This disentanglement is achieved due to the linear coupling between variables on neighboring nodes, which is obtained by introducing auxiliary local fields  $\hat{\mathbf{h}}_i$ . A different but equivalent formulation of the dynamic cavity considers factor graphs in which the variable nodes contain pairs of trajectories, e.g.  $(\mathbf{x}_i, \mathbf{x}_j)$ , of sites that are neighbors on the underlying interaction graph. This is the formulation that leads to the BP method in Refs.[2, 12, 13].

According to this graphical model construction, the following *dynamic cavity equations* represent an ansatz for describing the stochastic dynamics associated with the dynamic partition function  $\mathcal{Z}$  on a tree-like interaction graph,

$$c_{ij} \left[ \mathbf{x}_i, \hat{\mathbf{h}}_i \right] = \frac{1}{\mathcal{Z}_{ij}} p(x_i^0) \prod_{t=0}^{T-1} \left[ \delta(\hat{h}_i^t - i) (1 - \varepsilon_i^t) (\delta_{x_i^{t+1}, x_i^t} - \delta_{x_i^{t+1}, 1}) + \delta(\hat{h}_i^t) \delta_{x_i^{t+1}, 1} \right] \\ \times \prod_{k \in \partial i \setminus j} \left\{ \int D\hat{\mathbf{h}}_k \sum_{\mathbf{x}_k} c_{ki} \left[ \mathbf{x}_k, \hat{\mathbf{h}}_k \right] e^{-i \sum_t (\hat{h}_i^t \nu_{ki}^t x_k^t + \hat{h}_k^t \nu_{ik}^t x_i^t)} \right\} \quad (\text{A7})$$

where  $\int D\hat{\mathbf{h}}_i = \prod_{t=0}^{T-1} \left[ \int_{-\infty}^{+\infty} d\hat{h}_i^t \right]$ . Then, using the Fourier transforms

$$c[\mathbf{x}, \mathbf{s}] = \prod_{t=0}^{T-1} \left[ \int_{-\infty}^{+\infty} d\hat{h}^t e^{-is^t \hat{h}^t} \right] c[\mathbf{x}, \hat{\mathbf{h}}] \quad (\text{A8})$$

$$c[\mathbf{x}, \hat{\mathbf{h}}] = \prod_{t=0}^{T-1} \left[ \int_{-\infty}^{+\infty} \frac{ds^t}{2\pi} e^{is^t \hat{h}^t} \right] c[\mathbf{x}, \mathbf{s}], \quad (\text{A9})$$

the dynamic cavity equations can be written as

$$c_{ij}[\mathbf{x}_i, \mathbf{s}_i] = \frac{1}{\mathcal{Z}_{ij}} p(x_i^0) \prod_{t=0}^{T-1} \left\{ \int_{-\infty}^{+\infty} d\hat{h}_i^t e^{-is_i^t \hat{h}_i^t} \left[ \delta(\hat{h}_i^t - i) (1 - \varepsilon_i^t) (\delta_{x_i^{t+1}, x_i^t} - \delta_{x_i^{t+1}, 1}) + \delta(\hat{h}_i^t) \delta_{x_i^{t+1}, 1} \right] \right. \\ \left. \times \prod_{k \in \partial i \setminus j} \left[ \sum_{\mathbf{x}_k} \int_{-\infty}^{+\infty} d\hat{h}_k^t \int_{-\infty}^{+\infty} \frac{ds_k^t}{2\pi} e^{is_k^t \hat{h}_k^t} c_{ki}[\mathbf{x}_k, \mathbf{s}_k] e^{-i(\hat{h}_i^t \nu_{ki}^t x_k^t + \hat{h}_k^t \nu_{ik}^t x_i^t)} \right] \right\}. \quad (\text{A10})$$

The expression can be simplified by performing the integrals over the auxiliary variables  $\{\hat{\mathbf{h}}_k\}_{k \in \partial i \setminus j}$  first,

$$c_{ij}[\mathbf{x}_i, \mathbf{s}_i] = \frac{1}{\mathcal{Z}_{ij}} p(x_i^0) \prod_{t=0}^{T-1} \left\{ \int_{-\infty}^{+\infty} d\hat{h}_i^t e^{-is_i^t \hat{h}_i^t} \left[ \delta(\hat{h}_i^t - i) (1 - \varepsilon_i^t) (\delta_{x_i^{t+1}, x_i^t} - \delta_{x_i^{t+1}, 1}) + \delta(\hat{h}_i^t) \delta_{x_i^{t+1}, 1} \right] \right. \\ \left. \times \prod_{k \in \partial i \setminus j} \left[ \sum_{\mathbf{x}_k} \int_{-\infty}^{+\infty} ds_k^t c_{ki}[\mathbf{x}_k, \mathbf{s}_k] e^{-i\hat{h}_i^t \nu_{ki}^t x_k^t} \int_{-\infty}^{+\infty} \frac{d\hat{h}_k^t}{2\pi} e^{i\hat{h}_k^t (s_k^t - \nu_{ik}^t x_i^t)} \right] \right\} \quad (\text{A11a})$$

$$= \frac{1}{\mathcal{Z}_{ij}} p(x_i^0) \prod_{t=0}^{T-1} \left\{ \int_{-\infty}^{+\infty} d\hat{h}_i^t e^{-is_i^t \hat{h}_i^t} \left[ \delta(\hat{h}_i^t - i) (1 - \varepsilon_i^t) (\delta_{x_i^{t+1}, x_i^t} - \delta_{x_i^{t+1}, 1}) + \delta(\hat{h}_i^t) \delta_{x_i^{t+1}, 1} \right] \right. \\ \left. \times \prod_{k \in \partial i \setminus j} \left[ \sum_{\mathbf{x}_k} \int_{-\infty}^{+\infty} ds_k^t c_{ki}[\mathbf{x}_k, \mathbf{s}_k] e^{-i\hat{h}_i^t \nu_{ki}^t x_k^t} \delta(s_k^t - \nu_{ik}^t x_i^t) \right] \right\} \quad (\text{A11b})$$

then over the variables  $\{\mathbf{s}_k\}_{k \in \partial i \setminus j}$ ,

$$c_{ij}[\mathbf{x}_i, \mathbf{s}_i] = \frac{1}{\mathcal{Z}_{ij}} p(x_i^0) \prod_{t=0}^{T-1} \left\{ \int_{-\infty}^{+\infty} d\hat{h}_i^t e^{-is_i^t \hat{h}_i^t} \left[ \delta(\hat{h}_i^t - i) (1 - \varepsilon_i^t) (\delta_{x_i^{t+1}, x_i^t} - \delta_{x_i^{t+1}, 1}) + \delta(\hat{h}_i^t) \delta_{x_i^{t+1}, 1} \right] \right. \\ \left. \times \prod_{k \in \partial i \setminus j} \left[ \sum_{x_k^t} c_{ki}[\mathbf{x}_k, \boldsymbol{\nu}_{ik} \mathbf{x}_i] e^{-i\hat{h}_i^t \nu_{ki}^t x_k^t} \right] \right\} \quad (\text{A12a})$$

$$= \frac{1}{\mathcal{Z}_{ij}} p(x_i^0) \sum_{\mathbf{x}_{\partial i \setminus j}} \left\{ \left[ \prod_{k \in \partial i \setminus j} c_{ki}[\mathbf{x}_k, \boldsymbol{\nu}_{ik} \mathbf{x}_i] \right] \prod_{t=0}^{T-1} \left[ \int_{-\infty}^{+\infty} d\hat{h}_i^t e^{-i\hat{h}_i^t (s_i^t + \sum_{k \in \partial i \setminus j} \nu_{ki}^t x_k^t)} \right] \right. \\ \left. \times \left( \delta(\hat{h}_i^t - i) (1 - \varepsilon_i^t) (\delta_{x_i^{t+1}, x_i^t} - \delta_{x_i^{t+1}, 1}) + \delta(\hat{h}_i^t) \delta_{x_i^{t+1}, 1} \right) \right\} \quad (\text{A12b})$$

and finally over  $\hat{\mathbf{h}}_i$ , to obtain a more natural form for the dynamic cavity equations

$$c_{ij}[\mathbf{x}_i, \mathbf{s}_i] = \frac{1}{\mathcal{Z}_{ij}} p(x_i^0) \sum_{\mathbf{x}_{\partial i \setminus j}} \left\{ \left[ \prod_{k \in \partial i \setminus j} c_{ki}[\mathbf{x}_k, \boldsymbol{\nu}_{ik} \mathbf{x}_i] \right] \right. \\ \left. \times \prod_{t=0}^{T-1} \left[ \delta_{x_i^{t+1}, x_i^t} (1 - \varepsilon_i^t) e^{s_i^t + \sum_{k \in \partial i \setminus j} \nu_{ki}^t x_k^t} + \delta_{x_i^{t+1}, 1} \left( 1 - (1 - \varepsilon_i^t) e^{s_i^t + \sum_{k \in \partial i \setminus j} \nu_{ki}^t x_k^t} \right) \right] \right\}. \quad (\text{A13})$$

Due to the locality and independence of observations, the latter can then be included in the above equations as an additional single-node factor term, a local likelihood, to obtain the dynamic cavity equations in Eq. (11).

## Appendix B: Reduction to the time-forward equations in the absence of observations

A major consequence of the introduction of time-forward messages  $\rho_{\rightarrow t}^{i \setminus j}$  and time-backward messages  $\rho_{t \leftarrow}^{i \setminus j}$  is that, in the absence of observations, it is possible to prove that the quantities  $\mu_{i \setminus j}^t$  have to vanish for all edges  $\forall(i, j)$  and  $\forall t$  and then recover a purely time-forward dynamics.

Using the definition of  $m_{i \setminus j}^t$  by means of the quantities  $\rho_{\rightarrow t}^{i \setminus j}(x_i^t)$  and  $\rho_{t \leftarrow}^{i \setminus j}(x_i^t)$ , but performing the slicing one time step later, we obtain

$$m_{i \setminus j}^t = \frac{1}{\tilde{\mathcal{Z}}_{ij}} \sum_{x_i^t, x_i^{t+1}} \rho_{\rightarrow t}^{i \setminus j}(x_i^t) x_i^t M_{x_i^t x_i^{t+1}}^{i \setminus j} \rho_{t+1 \leftarrow}^{i \setminus j}(x_i^{t+1}) \quad (\text{B1a})$$

$$= \frac{1}{\tilde{\mathcal{Z}}_{ij}} \rho_{\rightarrow t}^{i \setminus j}(1) M_{t, 11}^{i \setminus j} \rho_{t+1 \leftarrow}^{i \setminus j}(1) \quad (1) \quad (\text{B1b})$$

or slicing one time step earlier,

$$m_{i \setminus j}^t = \frac{1}{\tilde{\mathcal{Z}}_{ij}} \sum_{x_i^{t-1}, x_i^t} \rho_{\rightarrow t-1}^{i \setminus j}(x_i^{t-1}) x_i^t M_{x_i^{t-1} x_i^t}^{i \setminus j} \rho_{t \leftarrow}^{i \setminus j}(x_i^t) \quad (\text{B2a})$$

$$= \frac{1}{\tilde{\mathcal{Z}}_{ij}} \left[ \rho_{\rightarrow t-1}^{i \setminus j}(1) M_{t-1, 11}^{i \setminus j} \rho_{t \leftarrow}^{i \setminus j}(1) + \rho_{\rightarrow t-1}^{i \setminus j}(0) M_{t-1, 01}^{i \setminus j} \rho_{t \leftarrow}^{i \setminus j}(1) \right]. \quad (\text{B2b})$$



Using the previous result it is possible to express  $m_{i \setminus j}^t$  as function of  $m_{i \setminus j}^{t-1}$

$$m_{i \setminus j}^t = m_{i \setminus j}^{t-1} + \frac{\rho_{\rightarrow t-1}^{i \setminus j}(0) M_{t-1,01}^{i \setminus j} \rho_{t \leftarrow}^{i \setminus j}(1)}{\tilde{Z}_{ij}} \times \frac{1 - m_{i \setminus j}^{t-1}}{1 - m_{i \setminus j}^{t-1}} \quad (\text{B3a})$$

$$= m_{i \setminus j}^{t-1} + \left(1 - m_{i \setminus j}^{t-1}\right) \left[ \frac{\rho_{\rightarrow t-1}^{i \setminus j}(0) M_{t-1,01}^{i \setminus j} \rho_{t \leftarrow}^{i \setminus j}(1)}{\rho_{\rightarrow t-1}^{i \setminus j}(0) M_{t-1,01}^{i \setminus j} \rho_{t \leftarrow}^{i \setminus j}(1) + \rho_{\rightarrow t-1}^{i \setminus j}(0) M_{t-1,00}^{i \setminus j} \rho_{t \leftarrow}^{i \setminus j}(0)} \right] \quad (\text{B3b})$$

$$= m_{i \setminus j}^{t-1} + \left(1 - m_{i \setminus j}^{t-1}\right) \left[ \frac{\left[1 - (1 - \varepsilon_i^{t-1}) e^{\sum_{k \in \partial i \setminus j} m_{k \setminus i}^{t-1} \nu_{ki}^{t-1}}\right] \rho_{t \leftarrow}^{i \setminus j}(1)}{\left[1 - (1 - \varepsilon_i^{t-1}) e^{\sum_{k \in \partial i \setminus j} m_{k \setminus i}^{t-1} \nu_{ki}^{t-1}}\right] \rho_{t \leftarrow}^{i \setminus j}(1) + (1 - \varepsilon_i^{t-1}) e^{\sum_{k \in \partial i \setminus j} m_{k \setminus i}^{t-1} \nu_{ki}^{t-1}} \rho_{t \leftarrow}^{i \setminus j}(0)} \right]}. \quad (\text{B3c})$$

As already stressed in the main text, the last expression does not represent a time-forward equation because the quantities  $\rho_{t \leftarrow}^{i \setminus j}(x_i^t)$  are computed backward in time from  $T$  to step  $t$ . Time-forward dynamics is recovered if the two time-backward messages are equal, which is expected to occur in the absence of observations at later times. To prove this, one can first notice that from (34e),  $\mu_{i \setminus j}^t = 0$  if the time-backward messages are equal, i.e. if  $\rho_{t+1 \leftarrow}^{i \setminus j}(0) = \rho_{t+1 \leftarrow}^{i \setminus j}(1)$ . In the absence of observations also the inverse implication is true: when the set of messages  $\mu_{i \setminus j}^t$  at time  $t$  are zero and there is no observation also at time  $t$ , then the corresponding time-backward messages  $\rho_{t \leftarrow}^{i \setminus j}(x_i^t)$  are also uniform. Let us start from the time  $T-1$ , because by construction  $\mu_{i \setminus j}^T = 0$ , then using (34e) with the final time condition  $\rho_{T \leftarrow}^{i \setminus j}(x_i^T) = p(O_i^T | x_i^T)$  we obtain

$$\mu_{i \setminus j}^t = \frac{1}{\tilde{Z}_{ij}} \rho_{\rightarrow t}^{i \setminus j}(0) M_{T-1,00}^{i \setminus j} (p(O_i^T | 0) - p(O_i^T | 1)). \quad (\text{B4})$$

If no observation is provided on the final time, then  $p(O_i^T | x_i^T) = 1$  for  $x_i^T = 0, 1$  and the numerator vanishes, that is  $\mu_{i \setminus j}^{T-1} = 0$ . Moreover,

$$\rho_{T-1 \leftarrow}^{i \setminus j}(x_i^{T-1}) = \sum_{x_i^T} M_{x_i^{T-1} x_i^T}^{i \setminus j} p(O_i^T | x_i^T) \quad (\text{B5a})$$

$$= M_{x_i^{T-1} 0}^{i \setminus j} + M_{x_i^{T-1} 1}^{i \setminus j} \quad (\text{B5b})$$

that is

$$\begin{aligned} \rho_{T-1 \leftarrow}^{i \setminus j}(0) &= (1 - \varepsilon_i^{T-1}) e^{\sum_{k \in \partial i \setminus j} m_{k \setminus i}^{T-1} \nu_{ki}^{T-1}} p(O_i^{T-1} | 0) + \left(1 - (1 - \varepsilon_i^{T-1}) e^{\sum_{k \in \partial i \setminus j} m_{k \setminus i}^{T-1} \nu_{ki}^{T-1}}\right) p(O_i^{T-1} | 1) \\ &= p(O_i^{T-1} | 0), \end{aligned} \quad (\text{B6})$$

$$\begin{aligned} \rho_{T-1 \leftarrow}^{i \setminus j}(1) &= e^{\sum_{k \in \partial i \setminus j} \nu_{ki}^{T-1} \mu_{k \setminus i}^{T-1}} p(O_i^{T-1} | 1) \\ &= p(O_i^{T-1} | 1), \end{aligned} \quad (\text{B7})$$

meaning that  $\rho_{T-1 \leftarrow}^{i \setminus j}(0) = \rho_{T-1 \leftarrow}^{i \setminus j}(1)$  if no observation is included at time  $T-1$ . In this way, the equality is guaranteed at time  $T-1$  and one can proceed by induction. By assuming that, in the absence of observations at times larger than  $t$ , the equality is valid for time  $t+1$ , i.e.  $\rho_{t+1 \leftarrow}^{i \setminus j}(0) = \rho_{t+1 \leftarrow}^{i \setminus j}(1) = \rho_{t+1 \leftarrow}^{i \setminus j}$  for all directed edges  $(i, j)$ , then one obtains that  $\mu_{i \setminus j}^t = 0$ . Computing the time-backward messages at time  $t$ ,

$$\rho_{t \leftarrow}^{i \setminus j}(x_i^t) = \sum_{x_i^t, x_i^{t+1}} M_{x_i^t x_i^{t+1}}^{i \setminus j} \rho_{t+1 \leftarrow}^{i \setminus j}(x_i^{t+1}) \quad (\text{B8a})$$

$$= \left(M_{x_i^t 0}^{i \setminus j} + M_{x_i^t 1}^{i \setminus j}\right) \rho_{t+1 \leftarrow}^{i \setminus j}, \quad (\text{B8b})$$

and using that all  $\mu_{k \setminus i}^t$  vanish,

$$\rho_{t \leftarrow}^{i \setminus j}(x_i^t) \propto \begin{cases} p(O_i^t | 0) & \text{if } x_i^t = 0, \\ p(O_i^t | 1) & \text{if } x_i^t = 1, \end{cases} \quad (\text{B9})$$

that is independent of the value of  $x_i^t$  if no observation occurs at time  $t$ . By induction, this is true for every time, as long as no observation is included. Hence, it is possible to conclude that, in the absence of observations, the equations (B3c) for the cavity marginals  $m_{i \setminus j}^t$  reduce to the more standard time-forward mean-field equations in Eqs. (41).

### Appendix C: Efficient implementation in the infection time representation

As an alternative to the generic efficient formulation presented in Section III in terms of transfer-matrix formalism, the complexity of Eqs. (25)-(26) can be reduced from the exponential (in the temporal length  $T$ ) to polynomial exploiting the non-recurrency of the SI dynamic - in which only configurations of the type  $\mathbf{x}_i = (0, \dots, 0, 1, \dots, 1)$  are allowed - by using a simpler representation in terms of infection times. A SI epidemic trajectory can be parameterized by a unique set of integer variables  $t_i$  (one for each node) representing the first time at which individual  $i$  is infected, and taking values in  $t_i \in \{0, \dots, T+1\}$ . The case  $t_i = 0$  corresponds to individual  $i$  being originally infected at the initial time, i.e. being a patient-zero of the epidemics. The other special case  $t_i = T+1$  models the scenario where individual  $i$  never gets infected during the dynamics (which formally corresponds to  $t_i = +\infty$ ). The trajectory  $\mathbf{x}_i$  can be simply expressed as  $x_i^t = \Theta[t - t_i]$ , where  $\Theta[x]$  is a Heaviside-step function, with the convention  $\Theta[0] = 1$ . After some algebra, and defining  $\tilde{\nu}_i^t = \log(1 - \varepsilon_i^t)$  we can rewrite Eqs. (25),(26) and (27) as follows:

$$m_{i \setminus j}^t = \frac{1}{\tilde{\mathcal{Z}}_{ij}} \sum_{t_i=0}^t p(\mathbf{O}_i | t_i) p_0(t_i) \left[ \prod_{r=0}^{t_i-2} e^{\tilde{\nu}_i^r + \sum_{k \in \partial i \setminus j} m_{k \setminus i}^r \nu_{ki}^r} \right] \left[ 1 - \mathbb{I}_{1 \leq t_i \leq T} e^{\tilde{\nu}_i^{t_i-1} + \sum_{k \in \partial i \setminus j} m_{k \setminus i}^{t_i-1} \nu_{ki}^{t_i-1}} \right] \prod_{s=t_i}^{T-1} e^{\sum_{k \in \partial i \setminus j} \nu_{ik}^s \mu_{k \setminus i}^s} \quad (\text{C1})$$

$$\begin{aligned} \mu_{i \setminus j}^t &= \frac{1}{\tilde{\mathcal{Z}}_{ij}} \sum_{t_i=t+2}^{T+1} p(\mathbf{O}_i | t_i) p_0(t_i) \left[ \prod_{r=0}^{t_i-2} e^{\tilde{\nu}_i^r + \sum_{k \in \partial i \setminus j} m_{k \setminus i}^r \nu_{ki}^r} \right] \left[ 1 - \mathbb{I}_{1 \leq t_i \leq T} e^{\tilde{\nu}_i^{t_i-1} + \sum_{k \in \partial i \setminus j} m_{k \setminus i}^{t_i-1} \nu_{ki}^{t_i-1}} \right] \prod_{s=t_i}^{T-1} e^{\sum_{k \in \partial i \setminus j} \nu_{ik}^s \mu_{k \setminus i}^s} + \\ &- \frac{\mathbb{I}_{0 \leq t \leq T-1}}{\tilde{\mathcal{Z}}_{ij}} p(\mathbf{O}_i | t+1) p_0(t+1) \left[ \prod_{r=0}^t e^{\tilde{\nu}_i^r + \sum_{k \in \partial i \setminus j} m_{k \setminus i}^r \nu_{ki}^r} \right] \prod_{s=t+1}^{T-1} e^{\sum_{k \in \partial i \setminus j} \nu_{ik}^s \mu_{k \setminus i}^s} \end{aligned} \quad (\text{C2})$$

$$\tilde{\mathcal{Z}}_{ij} = \sum_{t_i=0}^{T+1} p(\mathbf{O}_i | t_i) p_0(t_i) \left[ \prod_{r=0}^{t_i-2} e^{\tilde{\nu}_i^r + \sum_{k \in \partial i \setminus j} m_{k \setminus i}^r \nu_{ki}^r} \right] \left[ 1 - \mathbb{I}_{1 \leq t_i \leq T} e^{\tilde{\nu}_i^{t_i-1} + \sum_{k \in \partial i \setminus j} m_{k \setminus i}^{t_i-1} \nu_{ki}^{t_i-1}} \right] \prod_{s=t_i}^{T-1} e^{\sum_{k \in \partial i \setminus j} \nu_{ik}^s \mu_{k \setminus i}^s} \quad (\text{C3})$$

where the function  $p_0(t_i)$  is related to the probability of node  $i$  being a patient zero, namely

$$p_0(r) = \begin{cases} \gamma_i^0 & r = 0 \\ 1 - \gamma_i^0 & r > 0 \end{cases} \quad (\text{C4})$$

Notice how all the summations/products w.r.t. the infection times are now linear in  $T$ . Analogously, the likelihood term for each observations on node  $i$  (Eq. (6)) can be rewritten use this representation as

$$p(O_i^{\tau_{o_i}} | t_i) = \begin{cases} (1 - f_{\text{FPR}}) \theta[t_i - (\tau_{o_i} + 1)] + f_{\text{FNR}} \theta[\tau_{o_i} - t_i] & \text{if } O_i^{\tau_{o_i}} = 0 \\ f_{\text{FPR}} \theta[t_i - (\tau_{o_i} + 1)] + (1 - f_{\text{FNR}}) \theta[\tau_{o_i} - t_i] & \text{if } O_i^{\tau_{o_i}} = 1 \end{cases} \quad (\text{C5})$$

with  $p(\mathbf{O}_i | t_i) = \prod_{o_i \in \mathcal{O}_i} p(O_i^{\tau_{o_i}} | t_i)$ . Analogous expressions w.r.t. (C1)-(C3) can be derived for the single-node marginal  $m_i^t$  and its normalization  $\mathcal{Z}_i$ . An efficient computational scheme can be attained by updating all the cavities of a fixed node at once, and then performing a random shuffling on the order nodes are updated. Intuitively, the speed-up induced by this protocol is that the forward and backward contribution to each cavity message - say, on link  $(i, j)$  can be computed by removing the corresponding link contribution from the *site* term  $i$ . In order to clarify this point, let us define the following four quantities, for each node  $i$ :

$$\mathcal{R}_i^{\rightarrow}(t) = \tilde{\nu}_i^t + \sum_{k \in \partial i} m_{k \setminus i}^t \nu_{ki}^t \quad \mathcal{R}_i^{\leftarrow}(t) = \sum_{k \in \partial i} \nu_{ik}^t \mu_{k \setminus i}^t \quad (\text{C6})$$

$$K_i^{\rightarrow}(t) = \sum_{r=0}^{t-2} \mathcal{R}_i^{\rightarrow}(r), \quad K_i^{\leftarrow}(t) = \sum_{s=t}^{T-1} \mathcal{R}_i^{\leftarrow}(s) \quad (\text{C7})$$

Analogous definitions hold for each cavity  $i \setminus j$ , just by letting the above summations run over all the neighbors of node  $i$  but  $j$ . Eqs. (C6) have also a physical interpretation. For instance,  $\mathcal{R}_i^{\rightarrow}(t)$  is a mean-field approximation for the log-probability of node  $i$  not being infected at time  $t$  by none of its neighbors. The above definitions Eqs (C6)-(C7) allow one to re-write the update of the cavity equations in a more compact form:

$$\tilde{\mathcal{Z}}_{ij} = \sum_{t_i=0}^{T+1} p(\mathbf{O}_i | t_i) p_0(t_i) e^{K_{i \setminus j}^{\rightarrow}(t_i)} \left[ 1 - \mathbb{I}_{1 \leq t_i \leq T} e^{\mathcal{R}_{i \setminus j}^{\rightarrow}(t_i-1)} \right] e^{K_{i \setminus j}^{\leftarrow}(t_i)} \quad (\text{C8})$$

$$m_{i \setminus j}^t = \frac{1}{\tilde{\mathcal{Z}}_{ij}} \sum_{t_i=0}^t p(\mathbf{O}_i | t_i) p_0(t_i) e^{K_{i \setminus j}^{\rightarrow}(t_i)} \left[ 1 - \mathbb{I}_{1 \leq t_i \leq T} e^{\mathcal{R}_{i \setminus j}^{\rightarrow}(t_i-1)} \right] e^{K_{i \setminus j}^{\leftarrow}(t_i)} \quad (\text{C9})$$

$$\begin{aligned} \mu_{i \setminus j}^t &= \frac{1}{\tilde{\mathcal{Z}}_{ij}} \sum_{t_i=t+2}^{T+1} p(\mathbf{O}_i | t_i) p_0(t_i) e^{K_{i \setminus j}^{\rightarrow}(t_i)} \left[ 1 - \mathbb{I}_{1 \leq t_i \leq T} e^{\mathcal{R}_{i \setminus j}^{\rightarrow}(t_i-1)} \right] e^{K_{i \setminus j}^{\leftarrow}(t_i)} \\ &\quad - \frac{1}{\tilde{\mathcal{Z}}_{ij}} p(\mathbf{O}_i | t+1) \mathbb{I}_{0 \leq t \leq T-1} p_0(t+1) e^{K_{i \setminus j}^{\rightarrow}(t+2) + K_{i \setminus j}^{\leftarrow}(t+1)} \end{aligned} \quad (\text{C10})$$

At fixed  $i$ , the quantities  $\mathcal{R}_{i \setminus j}^{\rightarrow}(t)$ ,  $\mathcal{R}_{i \setminus j}^{\leftarrow}(t)$ ,  $K_{i \setminus j}^{\rightarrow}(t)$ ,  $K_{i \setminus j}^{\leftarrow}(t)$  can be computed for each cavity by removing just one link contribution (i.e. the one corresponding to the link removed in that specific cavity graph), without further  $O(|\partial i|)$  computations, namely

$$\mathcal{R}_{i \setminus j}^{\rightarrow}(t) = \mathcal{R}_i^{\rightarrow}(t) - m_{j \setminus i}^t \nu_{ji}^t, \quad \mathcal{R}_{i \setminus j}^{\leftarrow}(t) = \mathcal{R}_i^{\leftarrow}(t) - \nu_{ij}^t \mu_{j \setminus i}^t \quad (\text{C11})$$

and similarly

$$K_{i \setminus j}^{\rightarrow}(t) = K_i^{\rightarrow}(t) - \sum_{r=0}^{t-2} m_{j \setminus i}^r \nu_{ji}^r, \quad K_{i \setminus j}^{\leftarrow}(t) = K_i^{\leftarrow}(t) - \sum_{s=t}^{T-1} \nu_{ij}^s \mu_{j \setminus i}^s \quad (\text{C12})$$

for any  $j \in \partial i$ . Furthermore, the computation Eqs. (C7) can be done recursively, in a forward (resp. backward) direction w.r.t. time for  $K_i^{\rightarrow}$  (resp.  $K_i^{\leftarrow}$ ), i.e. by exploiting

$$K_i^{\rightarrow}(t) = K_i^{\rightarrow}(t-1) + \mathcal{R}_i^{\rightarrow}(t-2), \quad K_i^{\leftarrow}(t) = K_i^{\leftarrow}(t+1) + \mathcal{R}_i^{\leftarrow}(t) \quad (\text{C13})$$

Clearly, equivalent relations hold for the link quantities  $K_{i \setminus j}^{\rightarrow(\leftarrow)}$ . Using all the above schemes, the overall computational cost to perform a single update of all the cavity quantities for a node  $i$  scales as  $O(|\partial i|T)$ . A further advantage of such a computational scheme is that the update of all the cavities for one node can be performed in parallel, a particularly convenient choice especially when dealing with dense graphs. The convergence criterion can be defined either w.r.t. the cavity messages  $\{m_{i \setminus j}^t\}$  and/or their conjugates  $\{\mu_{i \setminus j}^t\}$ , or eventually w.r.t. the single-site marginals  $\{m_i^t\}$ : the latter can be computed as

$$m_i^t = \frac{\sum_{t_i=0}^t p(\mathbf{O}_i | t_i) p_0(t_i) e^{K_i^{\rightarrow}(t_i)} \left[ 1 - \mathbb{I}_{1 \leq t_i \leq T} e^{\mathcal{R}_i^{\rightarrow}(t_i-1)} \right] e^{K_i^{\leftarrow}(t_i)}}{\sum_{t_i=0}^{T+1} p(\mathbf{O}_i | t_i) p_0(t_i) e^{K_i^{\rightarrow}(t_i)} \left[ 1 - \mathbb{I}_{1 \leq t_i \leq T} e^{\mathcal{R}_i^{\rightarrow}(t_i-1)} \right] e^{K_i^{\leftarrow}(t_i)}} \quad (\text{C14})$$

where the normalization is explicitly shown at the denominator. This expression is equivalent to Eq. (28) of the main text but rewritten using the infection-time representation just discussed.

#### Appendix D: Derivation of SCDC on the SIR model

In a Susceptible-Infected-Recovered (SIR) model, the possible individual states are  $x_i^t \in \{S, I, R\}$  and the transition probabilities between states are given by

$$W_i[x_i^{t+1} = S | \mathbf{x}^t] = \delta_{x_i^t, S} (1 - \varepsilon_i^t) \prod_{j \in \partial i} [1 - \lambda_{ji}^t \delta_{x_j^t, I}] \quad (\text{D1})$$

$$W_i[x_i^{t+1} = I | \mathbf{x}^t] = \delta_{x_i^t, I} (1 - r_i^t) + \delta_{x_i^t, S} \left[ 1 - (1 - \varepsilon_i^t) \prod_{j \in \partial i} [1 - \lambda_{ji}^t \delta_{x_j^t, I}] \right] \quad (\text{D2})$$

$$W_i[x_i^{t+1} = R | \mathbf{x}^t] = \delta_{x_i^t, R} + \delta_{x_i^t, I} r_i^t \quad (\text{D3})$$

where  $r_i^t$  is the recovery probability of individual  $i$  at time  $t$  and  $\lambda_{ij}^t$  is the probability that  $i$  transmits the infection to  $j$  at time  $t$ . As for the SI model, it is convenient to introduce a set of local fields  $h_i^t$  defined by

$$h_i^t = \sum_j \delta_{x_j^t, I} \nu_{ji}^t \quad (\text{D4})$$

in order to disentangle the interaction between individual  $i$  and its neighbors. The dynamical partition function of the system (neglecting observations for simplicity) is therefore

$$\begin{aligned} \mathcal{Z} &= \sum_{\mathbf{X}} \prod_i p(x_i^0) \prod_t \int dh_i^t \left\{ \delta_{x_i^{t+1}, S} W[x_i^{t+1} = S | \mathbf{x}^t] + \delta_{x_i^{t+1}, I} W[x_i^{t+1} = I | \mathbf{x}^t] + \right. \\ &\quad \left. + \delta_{x_i^{t+1}, R} W[x_i^{t+1} = R | \mathbf{x}^t] \right\} \delta \left( h_i^t - \sum_j \delta_{x_j^t, I} \nu_{ji}^t \right) \end{aligned} \quad (\text{D5a})$$

$$\begin{aligned} &= \sum_{\mathbf{X}} \prod_i p(x_i^0) \prod_t \int dh_i^t \left\{ \delta_{x_i^{t+1}, S} \delta_{x_i^t, S} (1 - \varepsilon_i^t) e^{h_i^t} + \delta_{x_i^{t+1}, I} \left[ \delta_{x_i^t, I} (1 - r_i^t) + \delta_{x_i^t, S} \left( 1 - (1 - \varepsilon_i^t) e^{h_i^t} \right) \right] + \right. \\ &\quad \left. + \delta_{x_i^{t+1}, R} \left( \delta_{x_i^t, R} + \delta_{x_i^t, I} r_i^t \right) \right\} \delta \left( h_i^t - \sum_j \delta_{x_j^t, I} \nu_{ji}^t \right) \end{aligned} \quad (\text{D5b})$$

$$\begin{aligned} &= \sum_{\mathbf{X}} \prod_i p(x_i^0) \prod_t \int dh_i^t \left\{ \delta_{x_i^{t+1}, S} \delta_{x_i^t, S} (1 - \varepsilon_i^t) e^{h_i^t} + \delta_{x_i^{t+1}, I} \left[ \delta_{x_i^t, I} (1 - r_i^t) + \delta_{x_i^t, S} \left( 1 - (1 - \varepsilon_i^t) e^{h_i^t} \right) \right] + \right. \\ &\quad \left. + \delta_{x_i^{t+1}, R} \left( \delta_{x_i^t, R} + \delta_{x_i^t, I} r_i^t \right) \right\} \int \frac{d\hat{h}_i^t}{2\pi} e^{i\hat{h}_i^t (h_i^t - \sum_j \delta_{x_j^t, I} \nu_{ji}^t)}. \end{aligned} \quad (\text{D5c})$$

Integrating over the local fields  $h_i^t$  for all times, we finally obtain the expression

$$\begin{aligned} \mathcal{Z} &= \sum_{\mathbf{X}} \int \mathcal{D}\hat{\mathbf{H}} \prod_i p(x_i^0) \prod_t \left\{ \delta(\hat{h}_i^t) \left[ \delta_{x_i^{t+1}, I} \left( \delta_{x_i^t, I} (1 - r_i^t) + \delta_{x_i^t, S} \right) + \delta_{x_i^{t+1}, R} \left( \delta_{x_i^t, R} + \delta_{x_i^t, I} r_i^t \right) \right] + \right. \\ &\quad \left. + \delta(\hat{h}_i^t - i) (1 - \varepsilon_i^t) \left[ \delta_{x_i^{t+1}, S} \delta_{x_i^t, S} - \delta_{x_i^{t+1}, I} \delta_{x_i^t, S} \right] \right\} \prod_{j>i} e^{\delta_{x_j^t, I} \nu_{ji}^t (-i\hat{h}_i^t) + \delta_{x_i^t, I} \nu_{ij}^t (-i\hat{h}_j^t)} \end{aligned} \quad (\text{D6})$$

which can in turn be interpreted as a graphical model in a similar way to what was done for the SI model. Inserting the observations and using Bayes theorem, it is then possible to obtain the corresponding expression for the posterior probability distribution and the following dynamic cavity equations for the SIR model with observations,

$$\begin{aligned} c_{ij}[\mathbf{x}_i, \hat{\mathbf{h}}_i] &= \frac{1}{\mathcal{Z}_{ij}} p(x_i^0) \prod_t \left\{ \delta(\hat{h}_i^t) \left[ \delta_{x_i^{t+1}, I} \left( \delta_{x_i^t, I} (1 - r_i^t) + \delta_{x_i^t, S} \right) + \delta_{x_i^{t+1}, R} \left( \delta_{x_i^t, R} + \delta_{x_i^t, I} r_i^t \right) \right] + \right. \\ &\quad \left. + \delta(\hat{h}_i^t - i) (1 - \varepsilon_i^t) \left[ \delta_{x_i^{t+1}, S} \delta_{x_i^t, S} - \delta_{x_i^{t+1}, I} \delta_{x_i^t, S} \right] \right\} p(O_i^t | x_i^t) \\ &\quad \times \prod_{k \in \partial i \setminus j} \sum_{\mathbf{x}_k} \int D\hat{\mathbf{h}}_k c_{ki}[\mathbf{x}_k, \hat{\mathbf{h}}_k] e^{\delta_{x_k^t, I} \nu_{ki}^t (-i\hat{h}_i^t) + \delta_{x_i^t, I} \nu_{ik}^t (-i\hat{h}_k^t)}. \end{aligned} \quad (\text{D7})$$

The expansion for small infection rates can be carried out similarly to the SI model, the only difference being that the average quantities are now defined as follows,

$$m_{i \setminus j}^t = \sum_{\mathbf{x}_i} \int D\hat{\mathbf{h}}_i c_{ij}[\mathbf{x}_i, \hat{\mathbf{h}}_i] \delta_{x_i^t, I} \quad (\text{D8})$$

$$\mu_{i \setminus j}^t = \sum_{\mathbf{x}_i} \int D\hat{\mathbf{h}}_i c_{ij}[\mathbf{x}_i, \hat{\mathbf{h}}_i] (-i\hat{h}_i^t). \quad (\text{D9})$$

With these definitions, approximating at first order and then re-exponentiating

$$\begin{aligned} c_{ij}[\mathbf{x}_i, \hat{\mathbf{h}}_i] &\approx \frac{1}{\mathcal{Z}_{ij}} p(x_i^0) \prod_t \left\{ \delta(\hat{h}_i^t) \left[ \delta_{x_i^{t+1}, I} \left( \delta_{x_i^t, I} (1 - r_i^t) + \delta_{x_i^t, S} \right) + \delta_{x_i^{t+1}, R} \left( \delta_{x_i^t, R} + \delta_{x_i^t, I} r_i^t \right) \right] \right. \\ &\quad \left. + \delta(\hat{h}_i^t - i) (1 - \varepsilon_i^t) \left[ \delta_{x_i^{t+1}, S} \delta_{x_i^t, S} - \delta_{x_i^{t+1}, I} \delta_{x_i^t, S} \right] \right\} \prod_t \left\{ e^{\sum_{k \in \partial i \setminus j} (-i\hat{h}_i^t m_{k \setminus i}^t \nu_{ki}^t + \delta_{x_i^t, I} \nu_{ik}^t \mu_{k \setminus i}^t)} p(O_i^t | x_i^t) \right\} \end{aligned} \quad (\text{D10})$$

where

$$\begin{aligned} \tilde{Z}_{ij} &= \sum_{\mathbf{x}_i} \int D\hat{\mathbf{h}}_i p(x_i^0) \prod_t \left\{ \delta(\hat{h}_i^t) \left[ \delta_{x_i^{t+1}, I} \left( \delta_{x_i^t, I} (1 - r_i^t) + \delta_{x_i^t, S} \right) + \delta_{x_i^{t+1}, R} \left( \delta_{x_i^t, R} + \delta_{x_i^t, I} r_i^t \right) \right] \right. \\ &\quad \left. + \delta(\hat{h}_i^t - i) (1 - \varepsilon_i^t) \left[ \delta_{x_i^{t+1}, S} \delta_{x_i^t, S} - \delta_{x_i^{t+1}, I} \delta_{x_i^t, S} \right] \right\} \prod_t \left\{ e^{\sum_{k \in \partial i \setminus j} (-i \hat{h}_i^t m_{k \setminus i}^t \nu_{ki}^t + \delta_{x_i^t, I} \nu_{ik}^t \mu_{k \setminus i}^t)} p(\mathcal{O}_i^t | x_i^t) \right\} \quad (\text{D11a}) \end{aligned}$$

$$\begin{aligned} &= \sum_{\mathbf{x}_i} p(x_i^0) \prod_t \left\{ \delta_{x_i^{t+1}, I} \left( \delta_{x_i^t, I} (1 - r_i^t) + \delta_{x_i^t, S} \right) + \delta_{x_i^{t+1}, R} \left( \delta_{x_i^t, R} + \delta_{x_i^t, I} r_i^t \right) \right. \\ &\quad \left. + (1 - \varepsilon_i^t) \left[ \delta_{x_i^{t+1}, S} \delta_{x_i^t, S} - \delta_{x_i^{t+1}, I} \delta_{x_i^t, S} \right] e^{\sum_{k \in \partial i \setminus j} m_{k \setminus i}^t \nu_{ki}^t} \right\} \prod_t \left\{ e^{\sum_{k \in \partial i \setminus j} \delta_{x_i^t, I} \nu_{ik}^t \mu_{k \setminus i}^t} p(\mathcal{O}_i^t | x_i^t) \right\}. \quad (\text{D11b}) \end{aligned}$$

Following the approach presented in Section III of the main text for the SI model, by defining the transfer matrix

$$\begin{aligned} M_{x_i^t x_i^{t+1}}^{i \setminus j} &= \left\{ \delta_{x_i^{t+1}, I} \left( \delta_{x_i^t, I} (1 - r_i^t) + \delta_{x_i^t, S} \right) + \delta_{x_i^{t+1}, R} \left( \delta_{x_i^t, R} + \delta_{x_i^t, I} r_i^t \right) \right. \\ &\quad \left. + (1 - \varepsilon_i^t) \left[ \delta_{x_i^{t+1}, S} \delta_{x_i^t, S} - \delta_{x_i^{t+1}, I} \delta_{x_i^t, S} \right] e^{\sum_{k \in \partial i \setminus j} m_{k \setminus i}^t \nu_{ki}^t} \right\} e^{\sum_{k \in \partial i \setminus j} \delta_{x_i^t, I} \nu_{ik}^t \mu_{k \setminus i}^t} p(\mathcal{O}_i^t | x_i^t), \quad (\text{D12}) \end{aligned}$$

the dynamical partition function Eq. (D11b) can be written as

$$\tilde{Z}_{ij} = \sum_{x_i} p(x_i^0) \left( \prod_{t=0}^{T-1} M_{x_i^t x_i^{t+1}}^{i \setminus j} \right) p(\mathcal{O}_i^T | x_i^T). \quad (\text{D13})$$

In matrix form, the quantity  $M_{x_i^t x_i^{t+1}}^{i \setminus j}$  of Eq. (D12) corresponds to Eq. (38) of the main text. Defining again forward and backward messages as

$$\rho_{\rightarrow t}^{i \setminus j}(x_i^t) = \sum_{x_i^0 \dots x_i^{t-1}} p(x_i^0) \prod_{t'=0}^{t-1} M_{x_i^{t'} x_i^{t'+1}}^{i \setminus j} = \sum_{x_i^{t-1}} \rho_{\rightarrow t-1}^{i \setminus j}(x_i^{t-1}) M_{x_i^{t-1} x_i^t}^{i \setminus j} \quad (\text{D14})$$

and

$$\rho_{t \leftarrow}^{i \setminus j}(x_i^t) = \sum_{x_i^{t+1} \dots x_i^T} \prod_{t'=t}^{T-1} M_{x_i^{t'} x_i^{t'+1}}^{i \setminus j} p(\mathcal{O}_i^T | x_i^T) = \sum_{x_i^{t+1}} \rho_{t+1 \leftarrow}^{i \setminus j}(x_i^{t+1}) M_{x_i^t x_i^{t+1}}^{i \setminus j} \quad (\text{D15})$$

which satisfy recursive equations analogous to Eqs. (33), we finally get, for the normalization  $\tilde{Z}_{ij}$  and the 1-time cavity messages  $m_{i \setminus j}^t, \mu_{i \setminus j}^t$ :

$$\tilde{Z}_{ij} = \sum_{x_i^t} \rho_{\rightarrow t}^{i \setminus j}(x_i^t) \rho_{t \leftarrow}^{i \setminus j}(x_i^t) = \rho_{\rightarrow t}^{i \setminus j}(S) \rho_{t \leftarrow}^{i \setminus j}(S) + \rho_{\rightarrow t}^{i \setminus j}(I) \rho_{t \leftarrow}^{i \setminus j}(I) + \rho_{\rightarrow t}^{i \setminus j}(R) \rho_{t \leftarrow}^{i \setminus j}(R) \quad (\text{D16})$$

and

$$m_{i \setminus j}^t = \sum_{\mathbf{x}_i} \int D\hat{\mathbf{h}}_i c_{ij}[\mathbf{x}_i, \hat{\mathbf{h}}_i] \delta_{x_i^t, I} \quad (\text{D17a})$$

$$= \frac{1}{\tilde{Z}_{ij}} \sum_{x_i^t} \rho_{\rightarrow t}^{i \setminus j}(x_i^t) \delta_{x_i^t, I} \rho_{t \leftarrow}^{i \setminus j}(x_i^t) \quad (\text{D17b})$$

$$= \frac{\rho_{\rightarrow t}^{i \setminus j}(I) \rho_{t \leftarrow}^{i \setminus j}(I)}{\tilde{Z}_{ij}} \quad (\text{D17c})$$

and

$$\mu_{i \setminus j}^t = \sum_{\mathbf{x}_i} \int D\hat{\mathbf{h}}_i c_{ij}[\mathbf{x}_i, \hat{\mathbf{h}}_i] \left( -i \hat{h}_i^t \right) \quad (\text{D18a})$$

$$= \frac{1}{\tilde{Z}_{ij}} \sum_{x_i^t, x_i^{t+1}} \rho_{\rightarrow t}^{i \setminus j}(x_i^t) (1 - \varepsilon_i^t) \left[ \delta_{x_i^{t+1}, S} \delta_{x_i^t, S} - \delta_{x_i^{t+1}, I} \delta_{x_i^t, S} \right] e^{\sum_{k \in \partial i \setminus j} m_{k \setminus i}^t \nu_{ki}^t + \delta_{x_i^t, I} \nu_{ik}^t \mu_{k \setminus i}^t} p(\mathcal{O}_i^t | x_i^t) \rho_{t+1 \leftarrow}^{i \setminus j}(x_i^{t+1}) \quad (\text{D18b})$$

$$= \frac{1}{\tilde{Z}_{ij}} \rho_{\rightarrow t}^{i \setminus j}(S) (1 - \varepsilon_i^t) e^{\sum_{k \in \partial i \setminus j} m_{k \setminus i}^t \nu_{ki}^t} p(\mathcal{O}_i^t | S) \left( \rho_{t+1 \leftarrow}^{i \setminus j}(S) - \rho_{t+1 \leftarrow}^{i \setminus j}(I) \right). \quad (\text{D18c})$$

### Appendix E: Example of normalization issue for leaves of the contact graph

The small coupling expansion requires to assume the normalization  $\mathcal{Z}_{ij}$  in (27), which sums over all the possible trajectories of node  $i$  assuming  $\mathbf{s}_i = 0$  at every time. The method thus considers all the trajectories in which the cavity node  $j$  is always susceptible, and therefore cannot infect node  $i$ . In particular, there are situations, such as the one considered in the example below, in which the normalization vanishes, meaning that it is not possible to explain an observed trajectory within the standard SI model. While this could seem pathological, it is worth stressing that the assumption done is necessary to obtain a message-passing algorithm that is independent of the trajectory of node  $j$ , a crucial condition to perform the expansion on which the present method is based. It is however possible to ensure that every trajectory of a node  $i$  remains feasible, the normalization constant being finite, by slightly modifying the epidemic model introducing a small self-infection probability. In addition to fix the normalization issue, a small value of self-infection probability does not deteriorate the predictive power of the method.

To better illustrate this problem, we consider a leaf node  $i$  and its unique neighbor  $j$ . In the cavity graph corresponding to the message  $c_{ij}[\mathbf{x}_i, \mathbf{s}_i]$ , node  $i$  will appear as an isolated node. As a consequence, it is expected that the approximation behind the SCDC equations cannot explain, within the cavity graph, an infection actually transmitted from node  $j$  to node  $i$ . Indeed, because of the absence of further neighbors, the normalization term reads

$$\tilde{\mathcal{Z}}_{ij} = \sum_{\mathbf{x}_i} p(x_i^0) \prod_{t=0}^{T-1} \left[ \left\{ \delta_{x_i^{t+1}, x_i^t} (1 - \varepsilon_i^t) + \delta_{x_i^{t+1}, 1} [1 - (1 - \varepsilon_i^t)] \right\} p(O_i^t | x_i^t) \right] p(O_i^T | x_i^T), \quad (\text{E1})$$

showing that an infection can only be explained by a self-infection event. When  $\varepsilon_i^t = 0$ , the cavity message admits trajectories for which node  $i$  is always susceptible or infected. When a repeated observation, at different time, were imply an infection event at some  $t \neq 0$ , the normalization would vanish, indicating an inconsistency in the model. This is prevented by the existence of a finite self-infection probability. Since it is recommended to operate in the limit of a vanishing self-infection, in the present case it is possible to analytically verify the limiting behavior for the cavity messages  $m_{i \setminus j}^t$  and  $\mu_{i \setminus j}^t$ .

As an example, we suppose that the leaf  $i$  is observed to be susceptible at time  $t_S$  and then is observed to be infected at time  $t_I > t_S$ . We consider a uniform self-infection probability  $\varepsilon_i^t = \varepsilon$  for any time  $t$  and any node  $i$ , and a uniform prior probability  $p(x_i^0 = 0) = 1 - \gamma$ ,  $p(x_i^0 = 1) = \gamma$ . The forward messages are

$$\rho_{\rightarrow t}^{i \setminus j}(x_i^t = 0) = \begin{cases} (1 - \gamma)(1 - \varepsilon)^t & \text{if } t \leq t_I, \\ 0 & \text{if } t > t_I, \end{cases} \quad (\text{E2})$$

$$\rho_{\rightarrow t}^{i \setminus j}(x_i^t = 1) = \begin{cases} \gamma + \varepsilon(1 - \gamma) \sum_{l=0}^{t-1} (1 - \varepsilon)^l & \text{if } t \leq t_S, \\ \varepsilon(1 - \gamma) \sum_{l=t_S}^{t-1} (1 - \varepsilon)^l & \text{if } t_S < t \leq t_I, \\ \varepsilon(1 - \gamma) \sum_{l=t_S}^{t_I-1} (1 - \varepsilon)^l & \text{if } t > t_I, \end{cases} \quad (\text{E3})$$

and the backward messages

$$\rho_{t \leftarrow}^{i \setminus j}(x_i^t = 0) = \begin{cases} \varepsilon(1 - \varepsilon)^{t_S-t} \sum_{l=0}^{t_I-1-t_S} (1 - \varepsilon)^l & \text{if } t \leq t_S, \\ \varepsilon \sum_{l=0}^{t_I-1-t} (1 - \varepsilon)^l & \text{if } t_S < t \leq t_I, \\ 1 & \text{if } t > t_I \end{cases} \quad (\text{E4})$$

$$\rho_{t \leftarrow}^{i \setminus j}(x_i^t = 1) = \begin{cases} 0 & \text{if } t \leq t_S, \\ 1 & \text{if } t > t_S. \end{cases} \quad (\text{E5})$$

The normalization factor taking into account the observations is

$$\tilde{\mathcal{Z}}_{ij} = \varepsilon(1 - \gamma) \sum_{l=t_S}^{t_I-1} (1 - \varepsilon)^l, \quad (\text{E6})$$

so that the cavity marginal is given by

$$m_{i \setminus j}^t = \begin{cases} 0 & \text{if } t \leq t_S, \\ \frac{\varepsilon(1 - \gamma) \sum_{l=t_S}^{t-1} (1 - \varepsilon)^l}{\varepsilon(1 - \gamma) \sum_{l=t_S}^{t_I-1} (1 - \varepsilon)^l} & \text{if } t_S < t \leq t_I, \\ 1 & \text{if } t > t_I. \end{cases} \quad (\text{E7})$$

In the limit of vanishing self-infection  $\varepsilon \rightarrow 0$ , the cavity marginal takes the simple expression

$$m_{i \setminus j}^t = \begin{cases} 0 & \text{if } t \leq t_S, \\ \frac{t-t_S}{t_I-t_S} & \text{if } t_S < t \leq t_I, \\ 1 & \text{if } t > t_I, \end{cases} \quad (\text{E8})$$

which gives a reasonable probability profile for the node  $i$  to be infected in the absence of node  $i$ . It is worth stressing that this is not the full marginal  $m_i^t$ , which also depends on the messages coming from  $j$  to  $i$ . The cavity field instead diverges for times  $t$  between the two observation times

$$\mu_{i \setminus j}^t = \begin{cases} 1 & \text{if } t \leq t_S, \\ -\infty & \text{if } t_S < t \leq t_I, \\ 0 & \text{if } t > t_I, \end{cases} \quad (\text{E9})$$

which is a clear consequence of having a vanishing normalization factor in the limit of zero self-infection. The divergence of the cavity field is thus the very non-physical effect of the inconsistency already discussed. In practice, in order to avoid divergences triggered by some peculiar combinations of observations, we then implement the algorithm using a cutoff  $\mu_{\text{cutoff}} < 0$  on the values of  $\mu_{i \setminus j}$ , such that the update rule (34e) is implemented as follows

$$\mu_{i \setminus j}^t = \max \left\{ \mu_{\text{cutoff}}, \frac{\rho_{\rightarrow t}^{i \setminus j}(0) M_{00}^{i \setminus j} \left( \rho_{t+1 \leftarrow}^{i \setminus j}(0) - \rho_{t+1 \leftarrow}^{i \setminus j}(1) \right)}{\rho_{\rightarrow t}^{i \setminus j}(0) \rho_{t \leftarrow}^{i \setminus j}(0) + \rho_{\rightarrow t}^{i \setminus j}(1) \rho_{t \leftarrow}^{i \setminus j}(1)} \right\}. \quad (\text{E10})$$